Streaming motion and population inversion of hot electrons in silver halides at crossed electric and magnetic fields*

Susumu Komiyama† and Taizo Masumi
Department of Pure and Applied Sciences, University of Tokyo, Komaba, Tokyo 153 Japan

Koji Kajita
Department of Physics, Faculty of Science, University of Tokyo, Bunkyo-ku, Tokyo 113 Japan
(Received 19 April 1979)

Galvanomagnetic measurements on photocarriers in pure AgCl and AgBr have been extended to an intense electric field ($E_x \sim 5$ kV/cm) and high magnetic field ($H_z \sim 58$ kOe) at 4.2 K by using a fast-pulse technique. Improved arrangements of blocking electrodes were adopted in order to detect simultaneously the three components of the transient photocurrent, Q_x, Q_y, and Q_z. Substantial roles of the LO-phonon emission in hot-electron kinetics have been revealed and clear pictures of the hot-electron phenomena in silver halides were obtained, for the first time, by a quantitative analysis of the results: (1) At $H_z = 0$, the momentum distribution of electrons (or holes) forms a line connecting the two points $\vec{v} = 0$ and $\vec{v} = (-V_{LO},0,0)$, where $(1/2)m^* V_{LO}^2 \equiv \hbar\omega_{LO}$, and the electrons are ideally streaming on the trajectory repeatingly emitting LO phonons. Hence, the electron drift velocity at high E_x at $H_z = 0$ is saturated to $(1/2)V_{LO}$. (2) An anomalous distribution of hot electrons involving population inversion predicted by Maeda and Kurosawa, is realized by applying a moderately high H_z such that $1 < \zeta < 2$, where $\zeta \equiv (2\hbar\omega_{LO}/m^*)^{1/2}(cE_x/H_z)^{-1}$. The distribution consists of two groups of electrons; the first group of electrons are streaming and the second group are accumulated within a high-energy area K in momentum space. Depending on the electron accumulation in the area K, the tangent of the Hall angle, $\tan\theta \equiv Q_y/Q_x$ and also Q_z increase abruptly with H_z. (3) It was found that the electron trapping lifetime varies with E_x and H_z. The streaming motion is responsible for the variation in lifetime. The experimental results here afford, for the first time, a set of conclusive evidence for the streaming motion, the anomalous distribution, and the advent of population inversion of the polarons in momentum space.

I. INTRODUCTION

Since Shockley and Ryder found a deviation from Ohm's law in the current-voltage characteristics in n-type Ge,[1] there have been a large number of investigations of hot-electron phenomena in semiconductors such as Ge, Si, InSb, and GaAs.[2] In the majority of these studies, the analysis is based on the assumption of a nearly isotropic distribution function for the hot-electron distribution. Further, in many of the articles, the simple term "hot-electron temperature" is utilized to characterize the hot-electron distribution which includes an implicit assumption of a displaced Maxwellian distribution. The assumption of a nearly isotropic distribution may be applicable to a hot-electron system in which the dominant scattering mechanism is of a nearly isotropic and quasielastic character (acoustical-phonon scattering being the case). The concept of hot-electron temperature may be well defined if electron-electron scattering is sufficient enough to randomize the momentum and the energy distributions among carriers. Although there often remains room for doubt concerning the actual applicability of these assumptions to a real hot-electron system, such pictures of hot-electron phenomena are now very familiar to us.

On the other hand, we can imagine a quite different type of hot electron phenomena, in which the LO-phonon emission by electrons plays an essential role both in the momentum relaxation and in the energy dissipation of hot electrons giving a highly anisotropic distribution function of hot electrons.[3,4] In this paper, we describe this type of hot electron phenomenon, in which the LO-phonon emission predominates all the other scattering mechanisms. Let us imagine an electron free from any scattering mechanisms except the LO-phonon emission. If one applies an electric field to the electron, the electron is accelerated by the field and readily acquires an energy enough to emit an LO-phonon. If the electron interacts strongly with LO-phonons, it will almost immediately emit an LO-phonon when it reaches the energy state $\epsilon = \hbar\omega_{LO}$ (where $\hbar\omega_{LO}$ is the LO-phonon energy). The electron is thereby scattered to a state near the ground state $\epsilon = 0$. Then the electron is accelerated again, and thereafter the same process repeats. This repeating motion is referred to as the "streaming motion." If the concentration of electrons is so low that the electron-electron scattering does not disturb the above repeating motion of each electron, the streaming motion is

possible for each electron and a needlelike distribution of the electrons results in the momentum space. Naturally the concept of hot-electron temperature loses its meaning. The streaming motion of electrons was first suggested by Shockley,[1] and subsequently investigated by several workers theoretically.[3,4] When one also applies a transverse magnetic field on the streaming electron, the kinetics of the streaming motion changes with the magnetic field. Vosilius and Levinson theoretically investigated the galvanomagnetic effects in the system of streaming electrons.[5] Further, a type of population inversion of hot electrons has been predicted by Maeda and Kurosawa[6] for an electron system interacting strongly with LO-phonons at crossed electric and magnetic fields. So far, few experimental works have been reported on these phenomena.[7] In this paper, we report the first experimental investigation on these phenomena.

There have been a considerable number of elementary investigations of the hot-electron effects in I-VII ionic materials such as silver, thallous, and alkali halides at helium temperatures.[8-14] In all the studies, a deviation from Ohm's law of photocurrents was observed in a high-electric-field range above 100–1000 V/cm. In spite of these investigations, we have not yet obtained a clear picture of the hot-electron kinetics in ionic materials. In particular, we have not yet known whether the LO-phonon emission occurs or not at high electric fields. Such an unsatisfactory situation of our knowledge about the hot electron phenomena in ionic materials comes from the lack of galvanomagnetic measurements at high electric fields in these materials. Recently, we have extended a cyclotron resonance experiment on photoelectrons in pure AgBr at helium temperatures to intense microwave fields (up to 3 kV/cm) at 35 GHz.[15-17] It was found that the width of the resonance line increases linearly with applied microwave field above ~100 V/cm giving a clear indication of the streaming motion of electrons. Detailed studies of galvanomagnetic effects of hot electrons (in static high electric field with transverse magnetic field) are required in order to obtain further information about the scattering mechanism and the momentum distribution of hot electrons. For this purpose, we have extended, in the present work, the galvanomagnetic measurements on photoelectrons in pure AgCl and AgBr crystals at helium temperatures to high electric fields (up to 5 kV/cm) and obtained definite evidences for the streaming motion of electrons in silver halides. Besides, for the first time we found the population inversion of hot electrons predicted by Maeda and Kurosawa.[6] It is the purpose of this paper to report thorough results of the galvanomagnetic experiments on photoelectrons (and photoholes) in zone refined crystals of AgCl and AgBr at 4.2 K in the range of electric fields up to 5 kV/cm and of magnetic fields up to 58 kOe. Based on a quantitative analysis of the experimental results, we give definite pictures of the hot electron kinetics in silver halides at helium temperature in the absence and in the presence of a transverse magnetic field.

Previously, we briefly reported on the streaming motion and also on the population inversion phenomena of hot electrons in silver halides.[18-20] In this paper, we include further results such as the electric and magnetic field dependence of the transient photocurrent vector. We will discuss the phenomena in detail on the basis of the thorough investigation. Section II begins with a brief survey of fundamental properties of AgCl and AgBr. Then the principle of the galvanomagnetic measurements and the experimental arrangements are described. In Sec. III, we present the experimental results on the vector components of the photocurrent Q_x, Q_y, and Q_z. Dependence of Q_x (the primary current) and of Q_y (the Hall current) on the magnetic field in the Ohmic region is presented in Sec. III A. The Hall mobility μ_H and the drift velocity v_d of electrons in the limit of low magnetic field are derived from the data of Q_x and Q_y as a function of electric field in Sec. III B. In Sec. III C, results of Q_x and Q_y at high electric fields and intense magnetic fields are presented. Subsequently, the currents Q_x and Q_y are transformed into two physically independent quantities; the tangent of the Hall angle, $\tan\theta \equiv Q_y/Q_x$, and the magnitude of the current, $(Q_x^2 + Q_y^2)^{1/2}$. Dependence of Q_z (the probe current along the magnetic field) on electric field and on magnetic field is presented in Sec. III D. All the results presented in Sec. III are discussed and interpreted in Sec. IV. In Sec. IV A, various scattering mechanisms are numerically estimated. In Secs. IV B to IV D, the streaming motion of electrons is quantitatively analyzed for both cases in the absence and in the presence of magnetic field, and the experimental results of μ_H, v_d, $\tan\theta$, Q_z, and $(Q_x^2+Q_y^2)^{1/2}$ are compared with the calculation.

II. EXPERIMENTAL METHODS

We begin with a brief review of fundamental properties of silver halides. AgCl and AgBr are I–VII ionic materials with an indirect band gap of 3.3 eV for AgCl,[21] and 2.7 eV for AgBr,[22] both at 4.2 K. The band structures of the two crystals are similar.[23,24] The lowest conduction band is of a simple standard form; namely, s-type with a

TABLE I. Properties of photocarriers in AgCl and AgBr crystals at 4.2 K. μ_0 is the Hall mobility at low electric field, τ^0_{imp} is the impurity scattering time for thermal carriers, p the energy exponent of the impurity scattering, τ_t the trapping lifetime,[a] and $n_{e,h}$ is the carrier concentration for a typical intensity of the excitation light. Values of μ_0, τ^0_{imp} and p were deduced from the data of Q_x and Q_y at low E_x. (See Sec. IIIA.) $n_{e,h}$ was roughly estimated from the magnitude of photosignals.

	Electron					Hole				
Specimen	μ_0 (cm^2/V sec)	τ^0_{imp} (psec)	p	τ_t (psec)	n_e (cm^{-3})	μ_0 (cm^2/V sec)	τ^0_{imp} (psec)	p	τ_t (psec)	n_h (cm^{-3})
AgCl *M*0-1	2.8×10^4	6.9	0			···	···	···	···	···
*MG*3-2	2.0×10^4	5.0	0	10–50	10^6–10^7	···	···	···	···	···
*M*1*CB*	3.8×10^4	9.5	$-\frac{1}{2}$			···	···	···	···	···
*M*1*CD*	1.5×10^4	3.7	0			···	···	···	···	···
AgBr *ZR*3-1	1.4×10^5	23	0			3.5×10^4	20	0		
*ZR*3-2	1.0×10^5	16	0	20–100	10^6–10^7	2.4×10^4	13.5	0	10–50	$\sim10^6$
C-157	4.1×10^4	6.8	0							

[a]Reference 38.

nondegenerate minimum at the point Γ in the Brillouin zone. The top of the valence band is located at the point L. The Hall mobility of conduction electrons μ_0 rises monotonically on cooling the crystal from room temperatures to 4.2 K.[8,25] The value of μ_0 at 4.2 K reaches a value of 10^4–10^5 cm^2/V sec in the zone refined crystals presently used (see Table I). The electron scattering at 4.2 K is dominated by impurities (in most of the crystals, ruled by neutral impurities as will be mentioned later). Holes are self-trapped in AgCl[26,27] but mobile in AgBr.[28] The value of the Hall mobility of holes in AgBr is as high as 10^4 cm^2/V sec (see Table I). Still the contribution of holes to the conduction is smaller than that of electrons by a factor 4–6. An electron in either crystal interacts strongly with LO-phonons and forms a polaron of an intermediate strength of coupling. The value of the effective ionic charge e^*/e (the Szigeti factor) and the coupling constant between the electron and the LO phonon α are listed in Table II. Values of the effective mass of an electron (electron polaron) and of a hole (hole polaron), both at the ground state, are also tabulated. The hole in AgBr has anisotropic mass parameters of a spheroidal symmetry.[28] There have been many theoretical calculations on the polaron energy spectrum (in the absence of external fields).[29-31] According to a Larsen's variational calculation,[31] the nonparabolicity of the polaron energy spectrum for $\alpha = 1.6$ (AgBr) is such that[32] $m_p^*(\epsilon = 0.2\hbar\omega_{LO})/m_p^*(0) \sim 1.05$ and $m_p^*(\epsilon = 0.5\hbar\omega_{LO})/$

TABLE II. Summary of fundamental properties of AgCl and AgBr. E_g denotes the indirect band gap at 4.2 K, e^*/e is the effective ionic charge, α is the coupling constant between electrons and LO phonons, and $\hbar\omega_{LO}$ is the LO-phonon energy at 4.2 K.

	Band edge[a]		E_g			$\hbar\omega_{LO}$	m_p^*	m_t^*	m_l^*
	Cond.	Valence	(eV)	e^*/e	α	(meV)	(electrons)[b]	(holes)[c]	
AgCl	Γ	L	3.3[d]	0.78	1.9[e]	23.0[f]	$0.43m_e$[g]		
AgBr	Γ	L	2.7[h]	0.73	1.6[e]	17.1[f]	$0.29m_e$[i]	$1.73m_e$[j]	$0.79m_e$[j]

[a]Reference 23.

[b]m_p^* is the "cold" electron-polaron mass determined by cyclotron resonance experiments, where m_e is the free-electron mass.

[c]$m_{t,l}^*$ are, respectively, the transverse and longitudinal mass of "cold" hole polaron.

[d]Reference 21.

[e]Reference 34.

[f]R. P. Lowndes, Phys. Lett. 21, 26 (1966).

[g]Reference 34 and H. Tamura and T. Masumi [J. Phys. Soc. Jpn. 30, 897 (1971)].

[h]Reference 22.

[i]References 34, 15, G. Ascarelli and F. C. Brown [Phys. Rev. Lett. 9, 209 (1962)], and H. Tamura and T. Masumi [J. Phys. Soc. Jpn. 30, 1763 (1971)].

[j]Reference 28.

$m_p^*(0) \sim 1.2$. This result is in substantial agreement with two independent results of the cyclotron resonance peak shift induced by raising resonance frequency[33] and by raising microwave power.[15,17] For further detailed description of the property of AgCl and AgBr, the reader is referred to several review articles.[34]

We now describe the method of the photoconductivity measurements for AgCl and AgBr crystals. The dark conductivity of these crystals is less than $10^{-20}(\Omega\,\mathrm{cm})^{-1}$ at helium temperatures. The crystals exhibit photoconductivity of the magnitude of $10^{-7}-10^{-9}(\Omega\,\mathrm{cm})^{-1}$ for typical illumination intensities. Because of the low conductivity of the crystals, the principle and the method of photoconductivity measurements in these materials are largely different from those applied to normal semiconducting materials. A fast pulse technique with blocking electrodes was used in this work. Some improvements were introduced in the arrangement of blocking electrodes to extend galvanomagnetic measurements to higher electric fields up to 5 kV/cm. Here we confine ourselves to a brief description of the principle and the method of experimental procedures for the modified blocking electrodes. For a detailed description of the fundamental principle of the photoconductivity measurement in insulating materials, the reader is referred to other papers.[34-36] Two types of blocking electrodes were adopted. Figure 1 shows the first type in which current components, Q_x and Q_y, of the photocurrent vector $\vec{Q}=(Q_x, Q_y, 0)$ in the presence of external fields $\vec{E}=(E_x, 0, 0)$ and $\vec{H}=(0, 0, H_z)$ are simultaneously detected. Figure 2 describes the second type in which Q_x and Q_z of the current vector $\vec{Q}=(Q_x, Q_y, Q_z)$ in the external fields $\vec{E}=(E_x, 0, E_z)$ and $\vec{H}=(0,0,H_z)$ are simultaneously detected. The first type of blocking electrodes (Fig. 1) is the type as first introduced by Iye and Kajita for the Hall effect measurements in CdS.[37] A specimen of a typical size $0.8\times 5\times 5$ mm is sandwiched between a lower metal electrode and a pair of upper metal electrodes. A quartz spacer of thickness about 0.9 mm is inserted between the specimen and the upper electrodes to improve uniformity of the electric field in the specimen. The specimen is insulated from the lower electrode by using a thin Mylar sheet. We can regard the specimen as the dielectric in a condenser and the electrodes as plates of the condenser. The upper electrodes are grounded through adequately high resistances. A voltage pulse with duration of 7 msec is applied to the lower electrode and the electric field E_x is produced in the specimen. Free carriers are excited in the specimen by an interband transition with a light pulse from a xenon flash tube (with

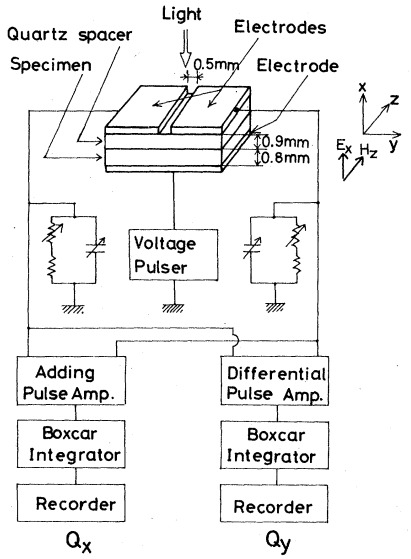

FIG. 1. Arrangement of blocking electrodes and the experimental apparatus for the measurement of Q_x and Q_y with $\vec{E}=(E_x, 0, 0)$ and $\vec{H}=(0, 0, H_z)$.

duration about 1 μsec) or a N_2 laser (with duration about 10 nsec) or from a dye laser (with duration about 10 nsec). The light pulse is synchronized to the electric field pulse. Intensity of the illumination is kept to a minimum by using fine mesh filters and glass filters. The photocarriers drift under the influence of applied field until they are captured by shallow traps. The trapping lifetime τ_t is as short as 10–100 psec at 4.2 K (Table I)[38] and is much shorter than the duration of the light pulse. The average distance of the drift mo-

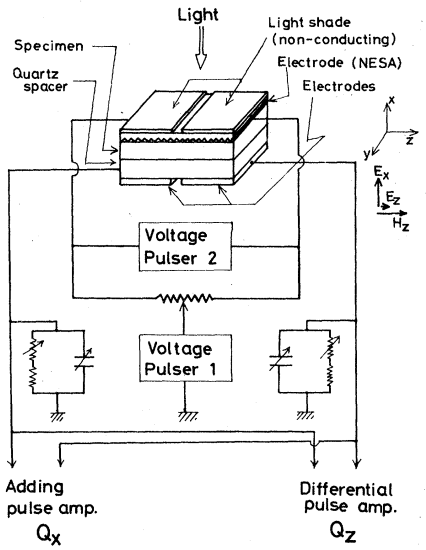

FIG. 2. Arrangement of blocking electrodes for the measurement of Q_x and Q_z with $\vec{E}=(E_x, 0, E_z)$ and $\vec{H}=(0, 0, H_z)$.

tion $v_d\tau_t$ (where v_d is the drift velocity) was estimated to be shorter than 20 μm in each crystal used, even at the highest electric field applied in the present experiment. Multitrapping effects are not involved in the electronic transport at 4.2 K. It is of great importance for the following analysis of experimental results that (i) the distance of the carrier drift is negligibly short as compared with the size of the specimen and (ii) the total number of photocarriers created by the light pulse N is sufficiently low so that the buildup of a space charge or an internal polarization field in the specimen can be ignored. The specimen is illuminated by infrared light after each pulse of excitation to sweep captured carriers out of trapped states. The measurement is repeated with a time interval ~600 msec. The sequence in time of pulse operation is shown in Fig. 3. A certain amount of charge is induced on the two upper electrodes by the drift of carriers through the image charge effect. The sum and the difference of the charges, Q^+ and Q^-, are simultaneously detected by an additive and a differential preamplifiers. Output signals are fed to Boxcar Integrators to improve the signal to noise ratio and recorded as a function of H_z or E_x. Here, the sum and the difference signals are proportional to the integrated currents along the x and y directions, Q_x and Q_y[39];

$$Q^+ = A^+ Q_x, \quad Q_x = -N\tau_t e v_x, \tag{1}$$

and

$$Q^- = A^- Q_y, \quad Q_y = -N\tau_t e v_y, \tag{2}$$

where e is the unit charge, A^+ and A^- are the sensitivity of the electrodes, N is the total number of carriers released by a pulse of light, τ_t the trapping lifetime, and v_x and v_y are the drift velocity along the x and y directions. (The carriers are assumed to be electrons.) Some modifications of the first type of electrodes are introduced in the second type of electrode arrangement (Fig. 2). Electric field E_x is set up by applying a voltage pulse between a resistance film electrode (NESA coated quartz plate) and a pair of lower metal electrodes. At the same time, a weak potential gradient is produced on the resistance film electrode. The potential gradient

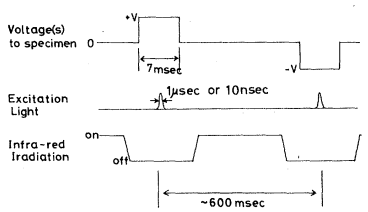

FIG. 3. Sequence in time of the pulse operation. The voltage pulses are alternately inverted to keep the buildup of space charge in the specimen to a minimum level.

provides a uniform electric field in the z direction E_z near the surface of the specimen. A strongly absorbed light penetrating a slit illuminates a thin area of the surface of the specimen so that the uniformity of both E_x and E_z is assured in the range where free carriers are excited. Experimental procedures for the second type of electrodes are the same as those described for the first type, while in this case,

$$Q^+ = A^+ Q_x, \quad Q_x = -N\tau_t e v_x, \tag{3}$$

and

$$Q^- = A^- Q_z, \quad Q_z = -N\tau_t e v_z, \tag{4}$$

where v_z denotes the drift velocity along the z direction (in the direction of magnetic field).

In both types of electrodes, the strength of electric field attained in the specimen along the x direction, E_x, was estimated in two independent ways. The first one is to calculate the electric field from the amplitude of applied voltage by taking into account the dielectric constants and the thicknesses of the specimen, the quartz spacer and the thin Mylar sheet. In the second way, the primary current Q_x was studied as a function of H_z by utilizing a standard arrangement of blocking electrodes,[10] and the Q_x-H_z curve at various levels of the strength of E_x was compared with that measured in the present arrangements. The results obtained in the two ways agreed well with each other.

In the transient condition, v_x and v_y which appear in Eqs. (1) and (2) have the following expressions for electrons in the limit of low electric field[35,36]:

$$v_x = -(e/m^*)\langle \tau/(1+\omega_c^2\tau^2)\rangle E_x \tag{5}$$

and

$$v_y = -(e/m^*)(e/m^*c)\langle \tau^2/(1+\omega_c^2\tau^2)\rangle H_z E_x, \tag{6}$$

where ω_c denotes the cyclotron angular frequency, $\omega_c \equiv eH_z/m^*c$, m^* is the effective mass of an electron, τ is the scattering time of the electron, e is the unit charge, and c is the light velocity. The drift velocity v_x which appears in Eq. (3) is also given by Eq. (5). The drift velocity v_z in Eq. (4) is given in the form[36]

$$v_z = -(e/m^*)\langle \tau \rangle E_z. \tag{7}$$

The bracket $\langle g \rangle$ means the statistical average over the distribution function; i.e.,

$$\langle g \rangle = \frac{1}{\Gamma(\frac{5}{2})} \int_0^\infty g x^{3/2} e^{-x} dx,$$

where $x \equiv \epsilon/kT$ with the energy of the electrons ϵ, the Boltzmann constant k, and the lattice temperature T. When the dependence of the scattering time on the electron energy is expressed in the

form

$$\tau = \tau_0 x^p , \tag{8}$$

Eqs. (5) and (6) can be calculated as a function of H_z with τ_0 and p as a parameter. As is well known, $p=0$ for neutral impurity scattering, $p=\frac{1}{2}$ for piezoelectric scattering, $p=-\frac{1}{2}$ for acoustical-phonon scattering, and $p=\frac{3}{2}$ for ionized impurity scattering. Let us define the Hall mobility μ_H for the transient condition as

$$\mu_H \equiv (c/H_z)\left|Q_y/Q_x\right| . \tag{9}$$

From Eqs. (1), (2), (5), and (6), the tangent of the Hall angle $\tan\theta \equiv Q_y/Q_x$ is expressed in the form

$$\tan\theta = \omega_c \langle\tau^2\rangle/\langle\tau\rangle . \tag{10}$$

Putting Eq. (10) into Eq. (9), we obtain

$$\mu_H = (e/m^*)\langle\tau^2\rangle/\langle\tau\rangle , \tag{11}$$

and hence

$$v_d \equiv \left|v_x(H_z=0)\right| = (\langle\tau\rangle^2/\langle\tau^2\rangle)\mu_H E_x . \tag{12}$$

In a later analysis, the absolute values of $\tan\theta$ at various values of E_x and H_z are discussed. As seen in relations (1) and (2), we directly measure the quantities Q^+ and Q^- (in the first type electrodes) which are proportional to Q_x and Q_y. It is necessary to know the ratio of the proportionality constants A^+/A^- in order to uniquely determine the value of $\tan\theta$ from the measurements of Q^+ and Q^-. First, as will be seen in Sec. IIIA, the energy exponent of the scattering, p, and the scattering time, τ_0, are determined by fitting the magnetic field dependence of Q^+ and Q^- signals at a low electric field to those calculated according to Eqs. (5) and (6). Then the absolute value of Q_y/Q_x (at the low electric field) is known from Eqs. (5) and (6) with the determined values of p and τ_0. By comparing the value of Q_y/Q_x with a directly measured value of Q^+/Q^-, we obtain the value of A^+/A^- to an accuracy of ±7%. Since the quantity A^+/A^- is believed to remain unchanged even when high electric fields or high magnetic fields are applied,[40] we can deduce the value of $\tan\theta$ at arbitrary strength of E_x and H_z from the data of Q^+ and Q^-. In Secs. III–V, we will present the corrected results Q_x and Q_y instead of the raw data of Q^+ and Q^-.

III. EXPERIMENTAL RESULTS

The origin of photocurrent was determined in two independent techniques: the Dember-effect and the Hall-effect measurements. Dominant carriers were confirmed to be electrons in all the AgCl and AgBr crystals. No indication of hole conduction was noted in AgCl crystals, whereas a small contribution from holes was recognized for AgBr crystals over the whole range of applied electric fields.

A. Dependence of Q_x and Q_y on magnetic field at the limit of low electric field

The acoustical-phonon scattering is believed to be relatively less important as compared with the impurity scattering at low electric fields.[41] The impurity scattering time ranges from 3 to 20 psec in the samples used, whereas the acoustical-phonon scattering time is estimated to be of several hundreds of psec at 4.2 K as shown in Fig. 4. In order to know the nature of impurity scattering, magnetic field dependences of Q_x and Q_y in the limit of low electric field were studied in some detail. Variation of the photocurrents Q_x and Q_y with H_z in AgCl $M0$-1 is plotted in Fig. 5. Both curves of $Q_x - H_z$ and $Q_y - H_z$ are best fitted to Eqs. (5) and (6) with the same parameters $p=0$ and $\tau_0 = 6.9$ psec. [Tabulated results of Dingle *et al.*[42] were used for the evaluation of the integrations in Eqs. (5) and (6).] In AgBr crystals, the curves of Q_x and Q_y can be well analyzed when a small contribution from holes ($\mu^h/\mu^e \sim 0.3$ and $\tau_t^h/\tau_t^e \sim 0.5$) is also taken into account. In order to analyze the two-carrier conduction, we adopted the expressions $Q_x = Ne(-\tau_t^e v_x^e + \tau_t^h v_x^h)$ and $Q_y = Ne(-\tau_t^e v_y^e + \tau_t^h v_y^h)$, and tried a curve fitting by taking τ_t^e, τ_t^h, τ_0^e, τ_0^h, and p^e, p^h as parameters. (The super-

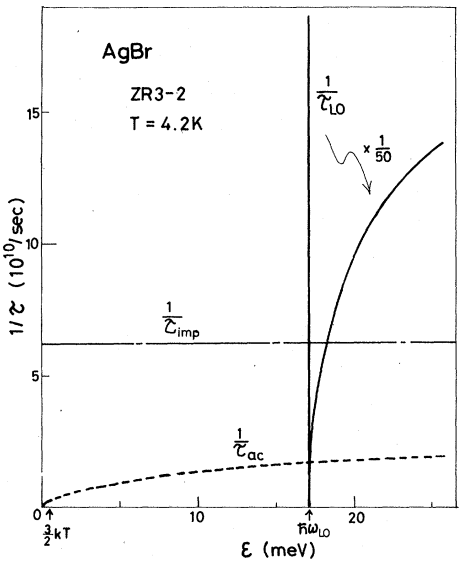

FIG. 4. Schematic description of the dependence of scattering rates of an electron on its energy ϵ. The broken line represents the impurity scattering rate in AgBr $ZR3$-2 crystal ($p=0$); the dotted line represents the acoustical-phonon scattering rate $\tau_{ac}^{-1}(\epsilon, T)$ at $T=4.2$ K and the solid line represents the scattering rate due to LO-phonon emission $\tau_{LO}^{-1}(\epsilon, T)$ at $T=4.2$ K.

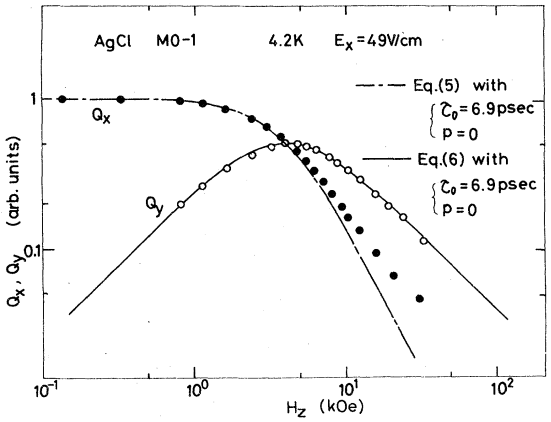

FIG. 5. Typical dependence of Q_x and Q_y on magnetic field in AgCl $M0$-1 crystal at 4.2 K at the limit of low E_x. The best fit to Eqs. (5) and (6) is obtained with the same parameters $p=0$ and $\tau_0=6.9\times10^{-12}$ sec.

scripts e and h denote electrons and holes.) We can obtain reasonable knowledge about the value of τ_t^h/τ_t^e, τ_0^h, p^e, and $\tau_0{}^e$, although a large arbitrariness remains for the value of p^h. As seen in Fig. 6, the Q_x and Q_y curves in AgBr $ZR3$-2 can be well interpreted when an appropriate contribution from holes is taken into account. The values of p and τ_0 were determined for all the crystals by the curve-fitting procedures[43] and the result is tabulated in Table I. In all the samples except AgCl $M1CB$, the value of p is 0 and accordingly the neutral impurity is believed to be the origin of the scattering. The scattering in AgCl $M1CB$ ($p=-\frac{1}{2}$) may be due to lattice defects of a large scale (such as dislocations).

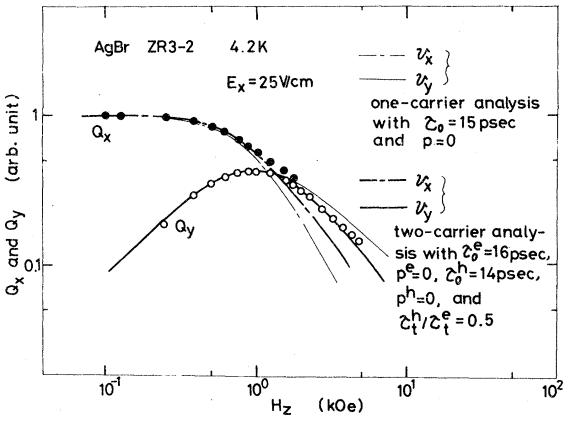

FIG. 6. Typical dependence of Q_x and Q_y on magnetic field in AgBr $ZR3$-2 crystal at 4.2 K at the limit of low E_x. Both curves are well analyzed when a small contribution from holes is taken into account.

B. Dependence of the drift velocity of electrons on electric field at the limit of low magnetic field

Photocurrents Q_x and Q_y were studied on all the AgCl and AgBr crystals as a function of $\vec{E}=(E_x, 0, 0)$ at a fixed low magnetic field $\vec{H}=(0, 0, H_z)$. The value of magnetic field H_z was typically 1kOe for AgCl crystals and 0.3 kOe for AgBr crystals. (The relation $\omega_c\tau_0 \ll 1$ is fulfilled in each sample.) The Hall mobility $\mu_H \equiv (c/H_z)|Q_y/Q_x|$ was calculated as a function of E_x from the data of Q_x and Q_y. Figure 7 illustrates the results obtained for AgCl crystals with those for AgBr crystals in the inset. In a relatively low electric field, μ_H decreases gradually with increasing electric field, while it decreases steeply with E_x at high electric fields. It should be noted that in the higher field range the sample dependence vanishes and all the data points converge to a single line with the slope of $E_x^{-1.0}$. If we simplify the equation (11), $\mu_H=(e/m^*)\tau$, we must consider that the scattering time of electrons τ decreases with E_x as $\tau \propto E_x^{-1.0}$. Electric field dependence of the Hall mobility of electrons was studied for AgBr by neglecting a small contribution from holes. Features of $\mu_H - E_x$ curves for AgBr crystals are essentially the same as those for AgCl crystals. The abrupt decrease in the Hall mobility suggests that the onset of LO-phonon emission takes place at high electric fields.

The drift velocity of electrons v_d was calculated

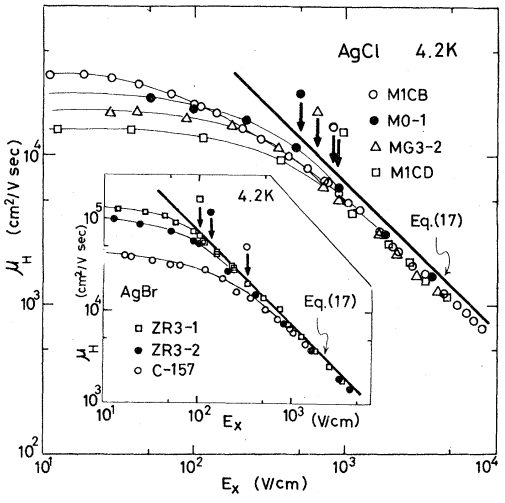

FIG. 7. Variation of the Hall mobility of electrons with E_x in different crystals of AgCl at 4.2 K. Sample dependence is reduced as E_x increases and is inversely proportional to E_x at high E_x. The inset shows the similar data for AgBr. Solid lines are drawn according to Eq. (17). The electric field at which $\tau_{imp}=T_{LO}$ is satisfied is indicated by an arrow for each crystal, where T_{LO} is defined by Eq. (16).

as a function of E_x from the observed value of μ_H by setting $\langle\tau\rangle^2/\langle\tau^2\rangle = 0.85$ for AgCl *M*1*CB* and $\langle\tau\rangle^2/\langle\tau^2\rangle = 1$ for the other crystals in Eq. (12).[44] The electric field dependence of v_d is compared with that of the primary photocurrent Q_x at $H_z = 0$ on different samples of AgCl in Figs. 8 and 9, where the position of the Q_x-E_x curve on the coordinates is chosen so that the data points of Q_x at the limit of low E_x agrees with v_d. In each sample, the electric field dependences of $v_d(E_x)$ and $Q_x(E_x)$ are characterized as follows: (a) In a relatively low electric field ($E_x \lesssim 300$ V/cm for AgCl *M*0-1 and $E_x \lesssim 700$ V/cm for AgCl *M*1*CB*), both v_d and Q_x increase together with E_x. The v_d-E_x and Q_x-E_x curves agree very well with each other in this range; (b) in a range of higher electric fields ($E_x \gtrsim 300$ V/cm for AgCl *M*0-1 and $E_x \gtrsim 700$ V/cm for AgCl *M*1*CB*), the increase in v_d is saturated whereas Q_x continues to increase, giving a large discrepancy between the $Q_x - E_x$ and $v_d - E_x$ curves. It was found in all the samples that the discrepancy between the $Q_x - E_x$ and $v_d - E_x$ curves emerges in the range of high electric fields where v_d is saturated. Similar data of Q_x and v_d for a crystal of AgBr are shown in Fig. 10. The saturation in v_d suggests again that the onset of the LO-phonon emission takes place at high electric fields. The departure of the $Q_x - E_x$ curve from the $v_d - E_x$ curve implies that the quantity $N\tau_t$ increases with E_x at high electric fields [see Eq. (1)]. In order to specify whether N increases or τ_t increases, we studied the

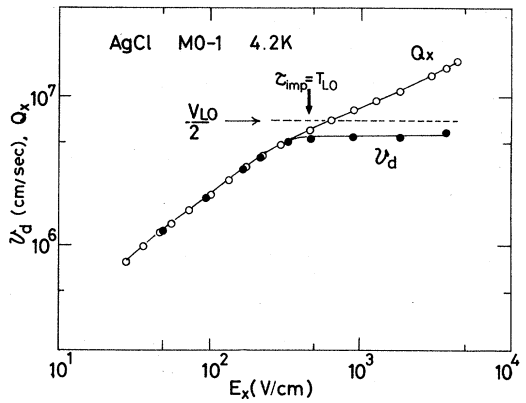

FIG. 8. Plot of photocurrent Q_x (open circles) and the drift velocity of electrons v_d (closed circles) in AgCl *M*0-1 at 4.2 K as a function of E_x. The drift velocity is calculated from the relation $v_d = \mu_H E_x$. Data points of Q_x represent the quantity $[\tau_t(E_x, 0)/\tau_t(0, 0)]v_d$ in the figure. The arrow indicates electric field at which $\tau_{imp} = T_{LO}$ is satisfied.

schubweg of the electron $v_d\tau_t$ as a function of E_x for the AgBr *ZR*3-2 crystal as follows. A strongly absorbed light from a N_2 laser ($\lambda = 3371$ Å) was used to create conduction electrons near the surface of the specimen, and the photocurrent magnitude ratio Q_x^f/Q_x^r was studied, where Q_x^f denotes the primary photocurrent when E_x is applied in the direction that the electron drifts into the specimen and Q_x^r for E_x in the opposite direction. (The absorption coefficient α for $\lambda = 3371$ Å is 700 cm^{-1}

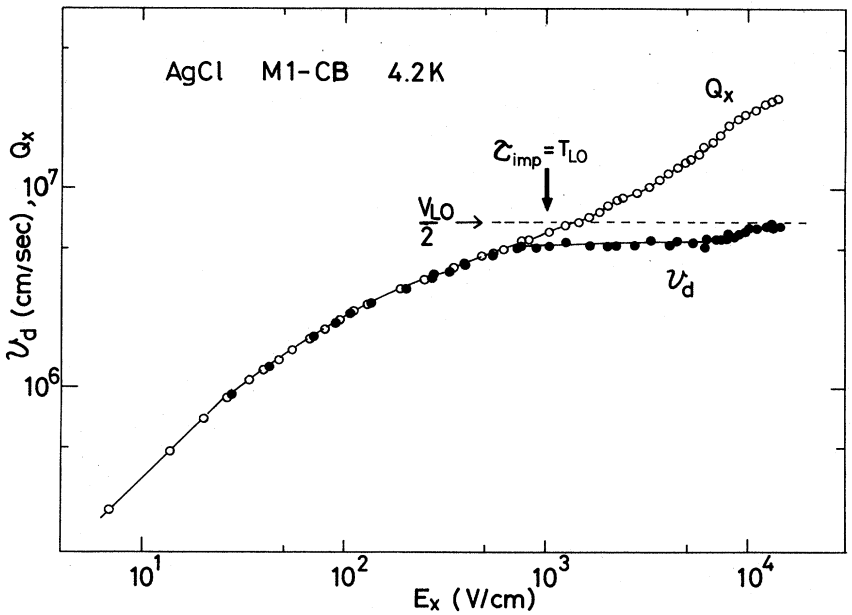

FIG. 9. Plot of photocurrent Q_x (open circles) and the drift velocity of electrons v_d (closed circles) as a function of E_x for AgCl *M*1*C*-*B* at 4.2 K. The arrow indicates the electric field at which $\tau_{imp} = T_{LO}$ is satisfied.

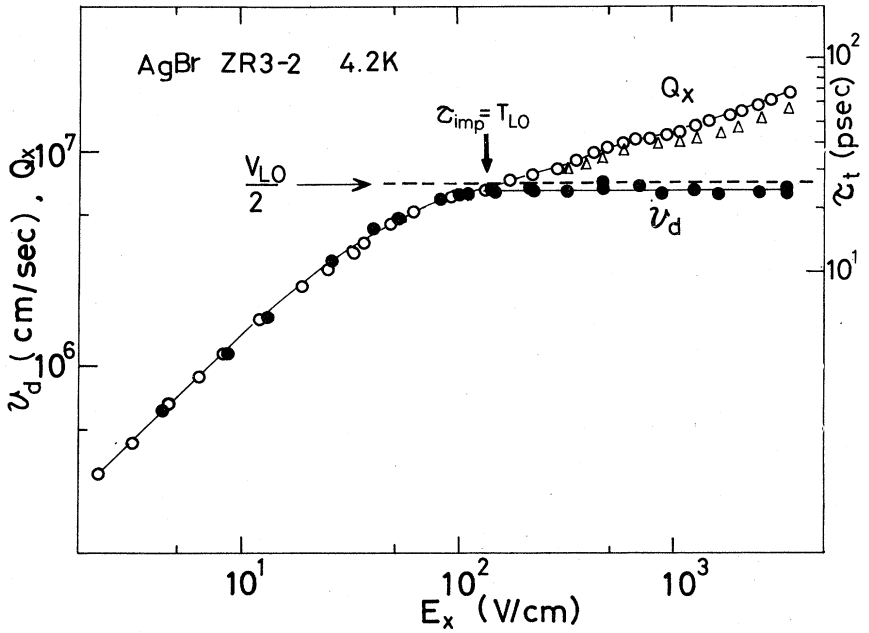

FIG. 10. Plot of photocurrent Q_x and the drift velocity of electrons v_d as a function of E_x for AgBr $ZR3$-2 at 4.2 K. Also, data points denoted by triangles show the variation in the trapping life-time τ_t with E_x, which was measured by using a forward and reverse technique of blocking electrons described in Sec. IIIB. The absolute value of τ_t is given on the scale at the right end of the figure.

for AgBr at 4.2 K.[45] When the thickness of the specimen d, the absorption coefficient α, and the *schubweg* $v_d\tau_t$ satisfy the relations, $d \gg \alpha^{-1}$ and $d \gg v_d\tau_t$ [as are fulfilled in the present experiment with $d = 800$ μm, $\alpha^{-1} = 14$ μm, and $v_d\tau_t < (5-10)\mu$m], the *schubweg* $v_d\tau_t$ is obtained from the relation[46] $v_d\tau_t = (|Q_x^f/Q_x^r| - 1)/\alpha$. It is believed that α is independent of E_x. The drift velocity v_d is almost constant in the high-electric-field range of interest; $v_d \sim \frac{1}{2}V_{LO}$. Thus we can deduce τ_t from the above measurement. Variation in τ_t with E_x is plotted with triangles in Fig. 10. The trapping lifetime τ_t increases with E_x just explaining the increase in Q_x. Thus the increase in Q_x at high electric fields is believed to be caused by the increase in τ_t with E_x.[47] On this basis, Q_x in Figs. 8–10 can be taken as the quantity $[\tau_t(E_x, 0)/\tau_t(0,0)]v_d$, where $\tau_t(E_x, 0)$ is the trapping lifetime at E_x and $H_z = 0$ and $\tau_t(0,0)$ represents the lifetime at low electric fields. (At low electric fields, τ_t is believed to be constant on application of H_z,[43] whereas it varies with H_z at high electric fields as will be discussed later.)

C. Dependnece of Q_x and Q_y on magnetic field at high electric fields

Photocurrents Q_x and Q_y were studied as a function of magnetic field $\vec{H} = (0, 0, H_z)$ at various levels of fixed electric field $\vec{E} = (E_x, 0, 0)$. The measurement was performed on all the samples. The data of Q_x and Q_y for AgCl $M0$-1 are plotted in Figs. 11 and 12 as a function of H_z with E_x as a parameter. Similar data for AgBr $ZR3$-2 are plotted in Figs. 13 and 14, where the vertical scales are chosen so that the data points represent the quantities $[\tau_t(E_x, H_z)/\tau_t(0,0)]v_x$ and $[\tau_t(E_x, H_z)/\tau_t(0,0)]v_y$.[48] As mentioned in Sec. IIIA, both curves of Q_x and Q_y at the limit of low E_x are well expressed by Eqs. (5) and (6). As E_x increases, the Q_x curve exhibits a shift toward higher magnetic field and the fall of the curve at high H_z region becomes steep. At the same time, the peak in the Q_y curve shifts toward higher magnetic field and becomes sharp. The line shapes of Q_x and Q_y at high electric fields can not be expressed by any means in the form of Eqs. (5) and (6). A thick arrow on each curve in Figs. 11–14 indicates the magnetic field H_z at which the relation $V_y = V_{LO}$ is satisfied, where V_y and V_{LO} are defined by

$$V_y \equiv cE_x/H_z \tag{13}$$

and

$$\tfrac{1}{2}m^*V_{LO}^2 \equiv \hbar\omega_{LO}\,, \tag{14}$$

with the light velocity c, the effective mass of the polaron $m^* = m_p^*$, and the LO-phonon energy $\hbar\omega_{LO}$ listed in Table II. For convenience, the values of

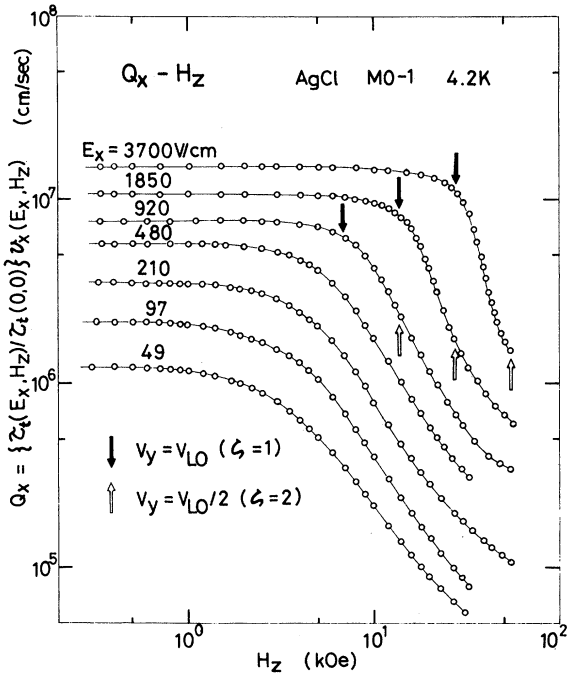

FIG. 11. Dependence of Q_x on magnetic field H_z at different values of E_x in AgCl $M0$-1. Data points of Q_x represent the quantity $[\tau_t(E_x,H_z)/\tau_t(0,0)]v_x(E_x,H_z)$. Black arrows indicate the magnetic fields at which $V_y = V_{LO}(\zeta = 1)$ is satisfied. White arrows indicate the magnetic fields at which $V_y = \frac{1}{2}V_{LO}$ $(\zeta = 2)$ is satisfied.

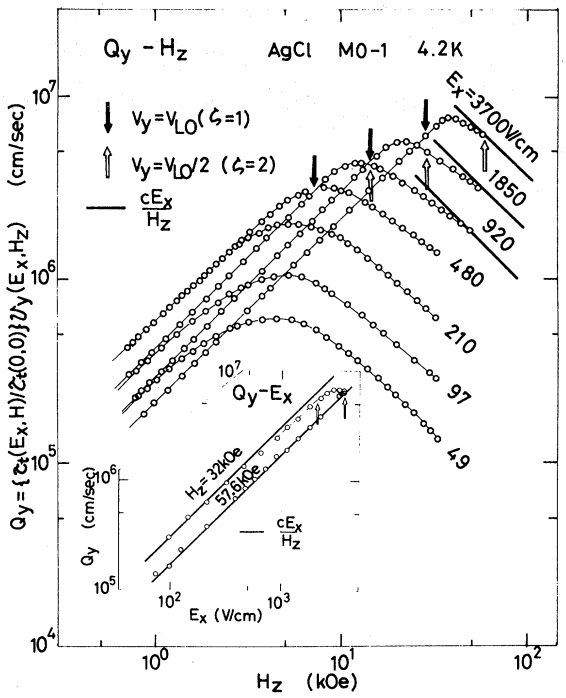

FIG. 12. Dependence of Q_y on magnetic field H_z at different values of E_x in AgCl $M0$-1. Data points represent the quantity $[\tau_t(E_x,H_z)/\tau_t(0,0)]v_y(E_x,H_z)$. The inset specifies the E_x dependence of Q_y at fixed high magnetic fields. Solid lines are drawn to indicate $v_y = V_y$ for the fixed high electric fields in the figure and for the fixed high magnetic fields in the inset.

V_{LO} for AgCl and AgBr are listed in Table III. The quantity V_y represents the velocity of an electron drifting along the y direction in crossed electric and magnetic fields in the absence of scattering. The quantity V_{LO} represents the velocity of an electron whose kinetic energy is equal to the LO-phonon energy. It should be noted that, for both the AgCl and AgBr crystals, the steep fall in the Q_x curves and the sharp peaks in the Q_y curves are observed just above the magnetic fields indicated by the thick arrows. These characteristics in the Q_x and Q_y curves were observed in all the other crystals of AgCl and AgBr. This suggests to us that a drastic change in the phenomena takes place in the higher magnetic field range where $V_y < V_{LO}$. Further, analogous behavior of the current due to positive holes is also suggested from the data on AgBr $ZR3$-2, namely, each Q_x curve at high electric field (Fig. 13) has a shoulder just above the magnetic field $V_y = V_{LO}^h$, which is indicated on each curve by an arrow with a superscript h. Here V_{LO}^h is defined by Eq. (14), where the averaged value of the effective mass for holes in AgBr, $(m_t^{*2}m_l^*)^{1/3} = 1.03m_e$, is used for m^*. The value of V_{LO}^h is also listed in Table III. Second, each Q_y curve has a slight hollow in the same range of H_z. Thus, we can believe that also the current components Q_z^h and Q_y^h due to holes have a steep fall and a sharp peak respectively where $V_y < V_{LO}^h$. (Note that the sign of the Hall current due to holes Q_y^h is inverse to that due to electrons. Accordingly, a sharp peak of Q_y^h curve may give rise to a hollow in the overall Q_y curve as just observed.)

Now, we transform the currents Q_x and Q_y into two quantities; the tangent of the Hall angle $\tan\theta \equiv Q_y/Q_x$ and the magnitude of the current $(Q_x^2 + Q_y^2)^{1/2}$.

1. Behavior of the Hall angle

The quantity $\tan\theta$ was calculated from the Q_x and Q_y data. It should be noted that $\tan\theta$ is a quantity that is not affected by the variation of the trapping lifetime of electrons. Figure 15 illustrates H_z dependence of $\tan\theta$ at various levels of E_x in AgCl $M0$-1. At low electric field ($E_x = 49$ V/cm), $\tan\theta$ increases linearly with H_z in a range of relatively low H_z. This means that the scattering time of electrons at low E_x stands constant on application of H_z [recall Eq. (10)]. The increase in $\tan\theta$ with H_z becomes dull having a

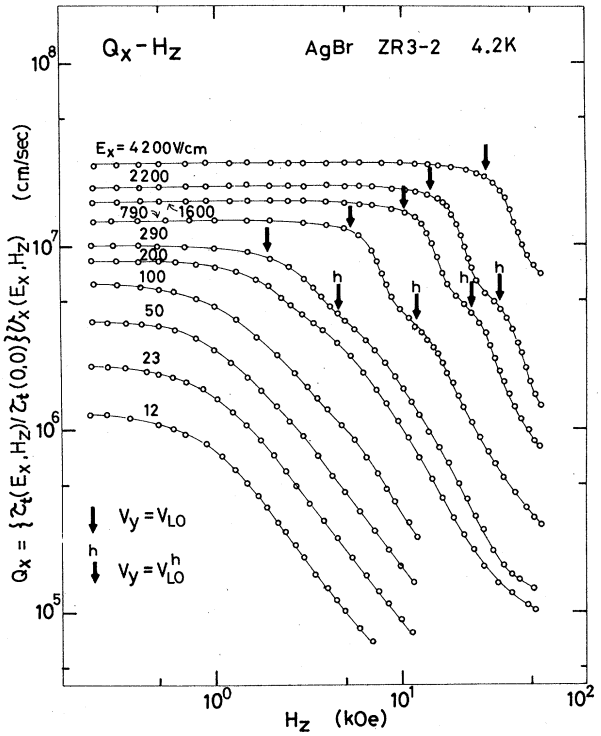

FIG. 13. Dependence of Q_x on magnetic field H_z at different values of E_x in AgBr $ZR3$-2. Black arrows indicate the magnetic fields at which $V_y = V_{LO}$ ($\zeta = 1$) is satisfied. Black arrows with superscript h indicate the magnetic fields at which $V_y^h = V_{LO}$ ($\zeta^h = 1$) is satisfied. Every Q_x-H_z curve at high E_x has a shoulder just above the field $V_y^h = V_{LO}$, reflecting a finite small contribution from holes.

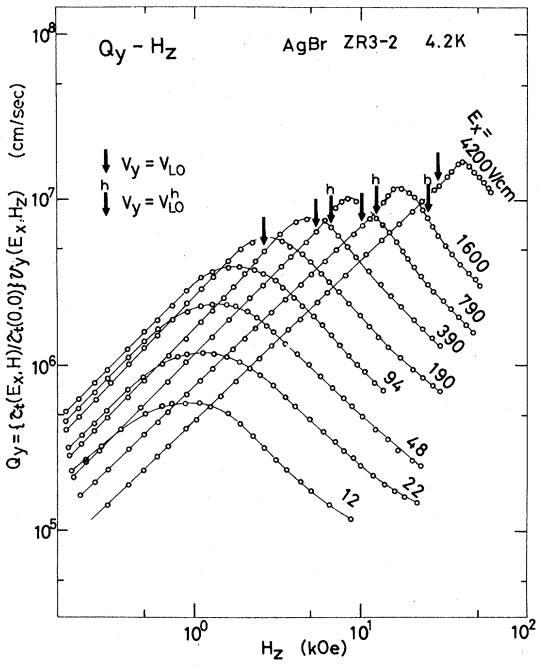

FIG. 14. Dependence of Q_y on magnetic field H_z at different values of E_x in AgBr $ZR3$-2. A small contribution from holes makes a slight hollow in a higher magnetic field range above $V_y^h = V_{LO}$ in each curve at high E_x.

tendency of saturation at high magnetic fields. By noting that the deviation $\tan\theta$ from the linear dependence on H_z becomes appreciable when $\tan\theta$ exceeds 1, we suggest that the deviation may be related to a quantization effect of the cyclotron orbit. {Note that the linear relation between $\tan\theta$ and H_z [Eq. (10)] was deduced classically on the assumption that $\tan\theta \ll 1$.} Even at high electric fields, $\tan\theta$ linearly increases with H_z in a range of relatively low magnetic fields, whereas it increases superlinearly with H_z above the magnetic field satisfying the relation $V_y = V_{LO}$. The data of $\tan\theta$ obtained on various crystals of AgCl at high electric fields are collected together in Fig. 16. Here, the electric fields are intense enough that v_d is saturated in each sample in the absence of magnetic field. In the figure, the data points are plotted as a function of a normalized field ζ.

$$\zeta \equiv V_{LO}/V_y = (2\hbar\omega_{LO}/m^*)^{1/2}(cE_x/H_z)^{-1}. \qquad (15)$$

First, in the region $\zeta < 1$, all the data points fall on a single line with a slope of $\zeta^{1.0}$. If we assume a simplifying relation of Eq. (10), $\tan\theta = \omega_c\tau$, the behavior of $\tan\theta$ in this range means that the

TABLE III. Characteristic quantities for streaming carriers. V_{LO} [defined by Eq. (14)] is the velocity of carriers whose kinetic energy is $\hbar\omega_{LO}$. T_{LO} [defined by Eq. (16)] is the time for a carrier to be accelerated from the ground state to reach a state of the LO-phonon energy. The evaluation of the quantities was made by using the values of m^* and $\hbar\omega_{LO}$ in Table II. The geometrically averaged value $(m_t^{*2}m_L^*)^{1/3} = 1.03m_e$ was used for holes in AgBr.

	Electron		Hole	
	V_{LO} (cm/sec)	T_{LO} at 1 kV/cm (psec)	V_{LO}^h (cm/sec)	T_{LO}^h at 1 kV/cm (psec)
AgCl	1.37×10^7	3.2	...	...
AgBr	1.45×10^7	2.2	7.73×10^6	4.2

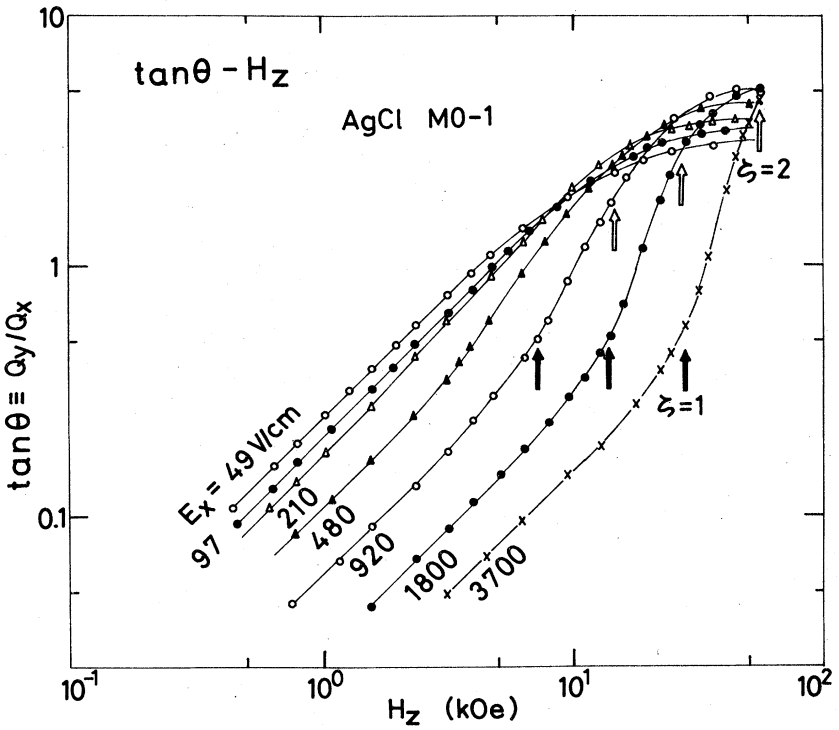

FIG. 15. Tangent of the Hall angle $\tan\theta \equiv Q_y/Q_x$ vs magnetic field at different values of E_x in AgCl $M0$-1. Black and white arrows indicate $\zeta = 1$ and $\zeta = 2$, respectively.

scattering time of an electron τ is inversely proportional to E_x and is independent of H_z in this range of ζ. Second, in the range $\zeta > 1$, every curve of $\tan\theta$ begins to depart from each other and to increase abruptly with increasing ζ. Similar data of $\tan\theta$ on the AgBr $ZR3$-2 crystal are shown in the inset of Fig. 16. One can find the same feature in the $\tan\theta - \zeta$ curves for AgBr as for AgCl but also note that the curves for AgBr have a kink at a higher ζ range which is absent in the curves for AgCl. The relation $\zeta^h = 1$ is satisfied at the kink, where ζ^h is defined by $\zeta^h \equiv V_{LO}/V_y^h$. The kink can be attributed to a contribution from the current due to holes, namely, it is believed that the tangent of the Hall angle of the hole current $\tan\theta^h \equiv Q_y^h/Q_x^h$ increases abruptly above $\zeta^h = 1$. (Note that $\tan\theta^h$ is opposite in sign to that for electrons.)

2. *Behavior of the magnitude of current*

The magnitude of current in the $x-y$ plane, $Q_{xy} \equiv (Q_x^2 + Q_y^2)^{1/2}$, were calculated from the Q_x and Q_y data. It should be noted that Q_{xy} is a quantity which explicitly reflects the variation in the trapping lifetime of electrons. Figure 17 illustrates the H_z dependence of Q_{xy} in AgCl $M0$-1 crystal at various values of E_x. The quantity Q_{xy} decreases rather smoothly with increasing H_z at a low electric field ($E_x = 49$ V/cm). The $Q_{xy} - H_z$ curve agrees well with the theoretical curve $Q_{xy} \propto (1 + \omega_c^2\tau^2)^{-1/2}$ obtained from Eqs. (5) and (6), indicating that the trapping lifetime τ_t is kept constant on application of H_z at low electric field. On the other hand, at high electric fields, Q_{xy} stands almost constant until it decreases abruptly above the magnetic field $V_y = V_{LO}$ ($\zeta = 1$). The data of Q_{xy} obtained on different crystals of AgCl at high electric fields are plotted together as a function of the normalized field ζ in Fig. 18. Let us note here that the data points of Q_{xy} in the figure represent the quantity $[\tau_t(E_x, H_z)/\tau_t(0,0)]v_{xy}$, where v_{xy} denotes $(v_x^2 + v_y^2)^{1/2}$. Differences between the positions of the data points of Q_{xy} and the indicated velocity $\frac{1}{2}V_{LO}$ at the left end of the figure reflect the increase in the lifetime of electrons (in respective samples) at given electric fields at $H_z = 0$. {Note that $\lim_{\zeta\to 0} Q_{xy} = [\tau_t(E_x, 0)/\tau_t(0,0)]v_{xy}$, where $v_{xy}(E_x, 0) = |v_x|$. Here, $|v_x|$ is saturated to $\frac{1}{2}V_{LO}$ as mentioned in Sec. III B.} All the data points of Q_{xy} begin to decrease with increasing ζ above 1, converging to a single line with the slope of $\zeta^{-1.0}$ in the range $\zeta > 2$.

D. Dependence of Q_z on electric and magnetic fields

Photocurrents Q_x and Q_z were studied as functions of magnetic field $\vec{H} = (0, 0, H_z)$ in the presence

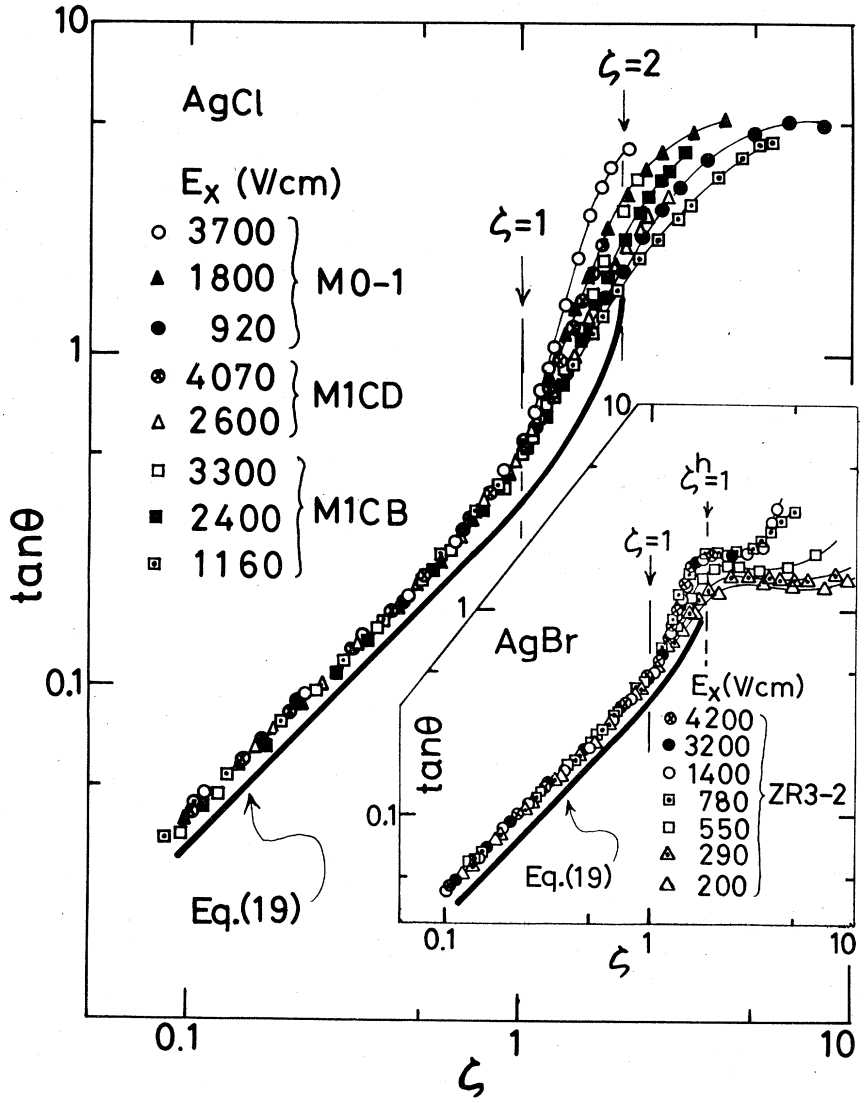

FIG. 16. Tangent of the Hall angle for AgCl as a function of ζ, where ζ is defined by Eq. (15). The inset shows the similar data for AgBr. In both AgCl and AgBr, all the data points for various crystals at several levels of high E_x add up to form a single line in the range $\zeta<1$, while they rise steeply departing each other in the range $\zeta>1$. The solid line is drawn according to Eq. (19) to be derived later.

of electric fields $\vec{E}=(E_x,0,E_z)$, where perturbing field E_z was fixed to $E_z=15$ V/cm and E_x was varied as a parameter. The measurements were performed on AgCl *M*1*CB* and AgBr *ZR*3-2. Equation (7) shows that v_z is a quantity which is not explicitly affected by H_z nor by E_x. Further, E_z ~15 V/cm is sufficiently low so that no hot electron effects are involved by E_z itself. (This is experimentally confirmed from the Ohmic relation $Q_x \propto E_x$ observed in the vicinity of E_x ~15 V/cm in Figs. 9 and 10.) On this basis, $Q_z(E_x,H_z)$ can be viewed as a "probe current" which reflects the mobility of the system at E_x and H_z. Variation of Q_z with H_z at various values of E_x are shown for AgCl *M*1*CB* in Fig. 19 and for AgBr *ZR*3-2 in Fig. 20. The current Q_z is proportional to the product of v_z and τ_t. (The quantity N is believed to be independent of external fields.[47]) We can obtain the value of $[\tau_t(E_x,H_z)/\tau_t(0,0)]v_z(E_z,H_z)$ from the data of $Q_z(E_x, H_z)$ by normalizing them with the low-field ($E_x=0$) data of Q_z. (The value of v_z at $E_x=0$ is known from the value of E_z and the value of low-field mobility of electrons in the crystal.) The coordinates of the figures represents the quantity $[\tau_t(E_x, H_z)/\tau_t(0,0)]v_z$. Characteristic features of the Q_z-H_z

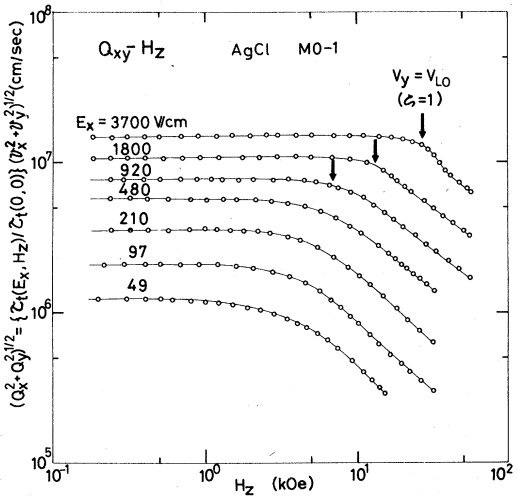

FIG. 17. Plot of the magnitude of current $Q_{xy} \equiv (Q_x^2+Q_y^2)^{1/2}$ against H_z at different values of E_x in AgCl $M0$-1. Data points of Q_{xy} represent the quantity $[\tau_t(E_x,H_z)/\tau_t(0,0)]\,(v_x^2+v_y^2)^{1/2}$.

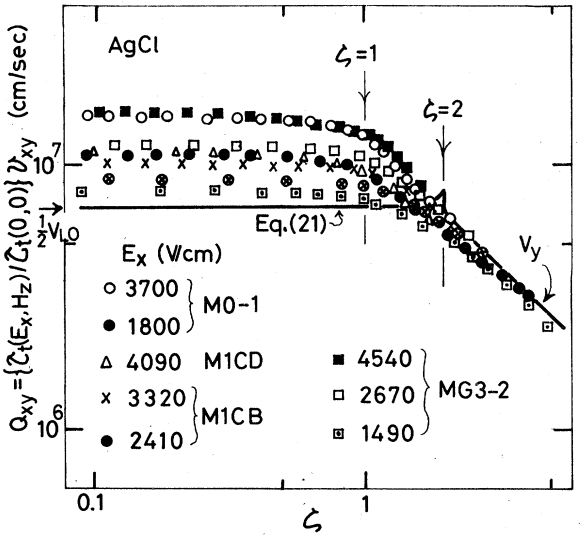

FIG. 18. Plot of Q_{xy} against ζ. The solid line in the range $\zeta<2$ is drawn according to Eq. (21) and the line in the range $\zeta>2$ represents the velocity V_y as a function of ζ.

curves for both crystals are summarized as follows:

(a) At $E_x=0$, Q_z stands almost constant up to the highest magnetic field. This means the absence of the longitudinal magnetoresistance effect in AgCl and AgBr, which is naturally expected for conduction electrons in these materials with a spherical energy surface.[23]

(b) At high E_x, the current Q_z stands constant to a low level up to the magnetic field satisfying $\zeta = 1$, whereas it begins to abruptly increase with further increasing H_z (in the range $\zeta>1$). At each high E_x, the current Q_z approaches to the zero E_x level, $Q_z(0,H_z)$, at an adequately high H_z (such that $\zeta>2$).

(c) At a fixed weak magnetic field, Q_z decreases monotonically with E_x.

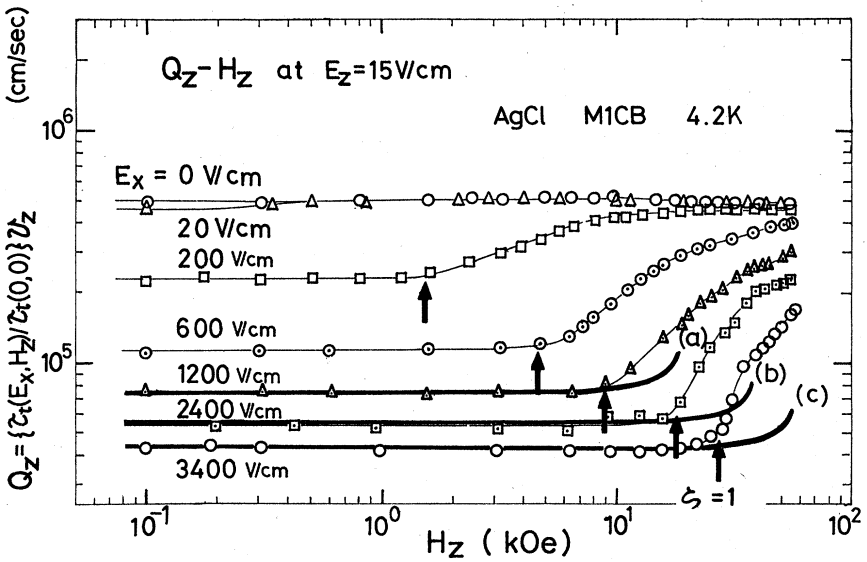

FIG. 19. Plot of the probe current Q_z in $\vec{E} = (E_x, 0, E_z)$ and $\vec{H} = (0, 0, H_z)$ in AgCl $M1C$-B at 4.2 K. E_z is fixed to 15 V/cm and E_x is varied as a parameter. Solid curves (a)–(c) are drawn according to Eq. (23) where E_x are, respectively, set to be 1200, 2400, and 3400 V/cm.

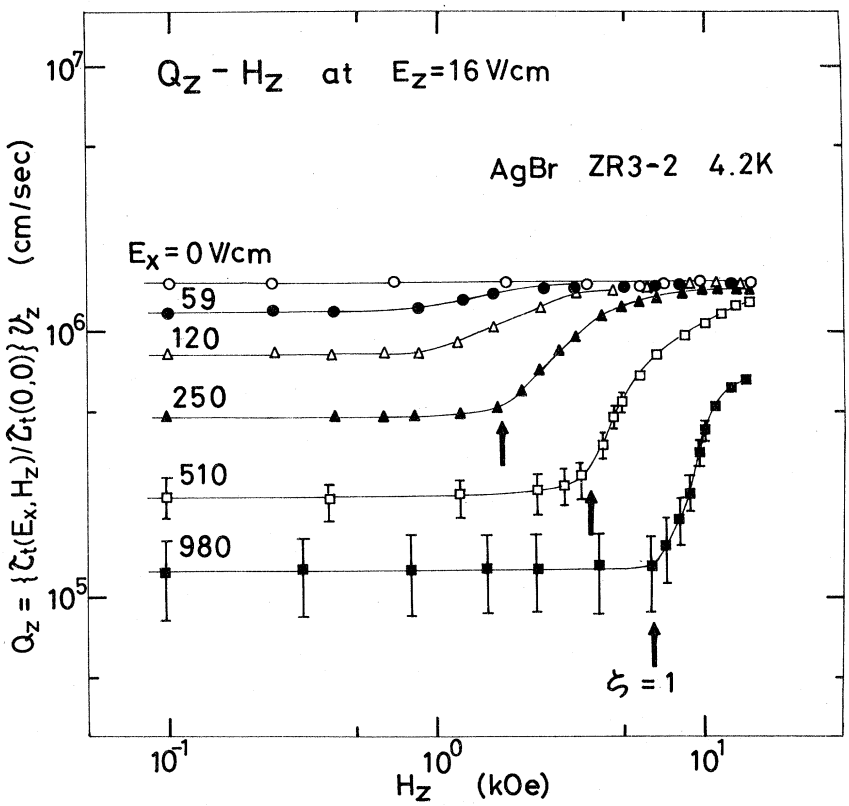

FIG. 20. Plot of the probe current Q_z in $\vec{E} = (E_x, 0, E_z)$ and $\vec{H} = (0, 0, H_z)$ in AgBr $ZR3$-2 at 4.2 K. E_z is fixed to 16 V/cm.

IV. DISCUSSION AND INTERPRETATION

A. Preliminary remarks

In the usual analysis of hot electron problems, a Maxwellian type of hot-electron distribution is often assumed. Such an assumption is not applicable to the present experiment since (i) the electron concentration of photocarriers is so low and (ii) the LO-phonon emission of electrons predominates all the other scattering mechanisms and it distorts severely the electron distribution function. With respect to assumption (i), the electron concentration was estimated from the magnitude of photosignals to be of the order of 10^6–10^7/cm^3. The momentum relaxation time due to electron-electron scattering τ_{e-e} is estimated to be as long as 10^{-5} sec for the carrier concentration of 10^7/cm^3 at 4.2 K, according to the Conwell-Weiskopf[49] or the Brooks-Herring[50] formulas. We should note that this value of τ_{e-e} is much longer than the trapping lifetime of electrons (see Table I). Thus we can neglect the intercarrier scattering; the phenomena in the present experiment are essentially those of *a single electron*. With respect to (ii), we have numerically estimated the relative importance of various scattering mechanisms.

The scattering rate of an electron in AgBr is shown as a function of the electron energy ϵ in Fig. 4. The impurity scattering, the acoustical phonon scattering and the LO-phonon scattering were considered. The impurity scattering rate τ_{imp}^{-1} is shown for the AgBr $ZR3$-2 crystal as a typical example. The rate of acoustical-phonon scattering $\tau_{\mathrm{ac}}^{-1}(\epsilon)$ was calculated according to the well-known form[51] $\tau_{\mathrm{ac}}(\epsilon, T)^{-1} = A[2n(\epsilon, T) + 1]\epsilon$, where $T = 4.2$ K and the constant A is set to be 4.8×10^{23} (erg sec)$^{-1}$ for AgBr[52] on the basis of Tamura's data[25] on the temperature dependence of the cyclotron resonance line. The phonon number $n(\epsilon, T)$ is given by $[\exp(\hbar c_s(2m^*\epsilon)^{1/2}/kT) - 1]^{-1}$, where k is the Boltzman constant, and $c_s = 2.96 \times 10^5$ cm/sec is the sound velocity.[53] The rate of LO-phonon scattering $\tau_{\mathrm{LO}}^{-1}(T, \epsilon)$ at 4.2 K was calculated according to the perturbation treatment[54];

$$\tau_{\mathrm{LO}}^{-1}(\epsilon, T) = 2\alpha\omega_{\mathrm{LO}}\left(\frac{\epsilon}{\hbar\omega_{\mathrm{LO}}}\right)^{-1/2} \times\left[N_{\mathrm{LO}}\sinh^{-1}\left(\frac{\epsilon}{\hbar\omega_{\mathrm{LO}}}\right)^{1/2} + (N_{\mathrm{LO}}+1)\sinh^{-1}\left(-1+\frac{\epsilon}{\hbar\omega_{\mathrm{LO}}}\right)^{1/2}\right],$$

where $\alpha = 1.6$ and the phonon number $N_{LO} = [\exp(\hbar\omega_{LO}/kT) - 1]^{-1}$ is practically zero at $T = 4.2$ K. It follows from $N_{LO} = 0$ that $\tau_{LO}^{-1}(\epsilon, 4.2\text{ K}) = 0$ for $\epsilon < \hbar\omega_{LO}$. As seen from Fig. 4, the feature of the scattering rate is quite different depending on whether ϵ is below or above $\hbar\omega_{LO}$. In the energy range $\epsilon < \hbar\omega_{LO}$, the scattering rate is low. The process of LO-phonon absorption is frozen out at low lattice temperatures. The acoustical-phonon scattering is not significant at 4.2 K. The dominant scattering mechanism is the impurity scattering. On the other hand, the scattering rate in the range $\epsilon > \hbar\omega_{LO}$ is enormously high due to the spontaneous emission of the LO phonon. With these situations, photoexcited electrons are confined in the energy states below $\hbar\omega_{LO}$ (or within the surface, $|\vec{v}| = V_{LO}$, in the velocity space) and a peculiar distribution of electrons results under the influence of external fields, as detailed in the following.

Problems of an anisotropic mass or the intervalley scattering are not involved in the following treatments, since the lowest conduction band in silver halides is of a standard form as noted at the begining of Sec. II. This enables us a simple analysis of the phenomena (except for the case of positive holes in AgBr). In the following analysis, we neglect, for simplicity, the effect of the nonparabolicity in the polaron energy spectrum.

B. Streaming motion of electrons at $H_z = 0$

Let us imagine that a free electron with an effective mass m^* is at rest at time $t = 0$ [$\vec{v}(0) = 0$]. At an electric field E_x applied with zero magnetic field, the electron will be accelerated along the x direction with the acceleration rate $\dot{v}_x = -eE_x/m^*$, and the velocity of the electron increases with time as $v_x(t) = -(eE_x/m^*)t$. The velocity reaches the value V_{LO} at the time $t = T_{LO}$, where T_{LO} is given by

$$T_{LO} \equiv (2m^*\hbar\omega_{LO})^{1/2}(eE_x)^{-1}. \tag{16}$$

Then, if the electron strongly interacts with the LO-phonon, it will almost immediately emit an LO-phonon, dissipating all of its kinetic energy thereby scattered to a state near the ground state $\vec{v} = 0$.[55] The scattered electron is again accelerated by the field and the above process repeats with the time interval of T_{LO}. The trajectory of such a streaming electron in the velocity space is expressed by a line $v_y = v_z = 0$ between the two points $v_x = 0$ and $v_x = -V_{LO}$ as illustrated in Fig. 21(a).

Here, let us consider the streaming motion of an electron taking into account the actual experimental situation. First, let us consider the life history of electrons. In the experiment, the electron is typically created at higher-energy states in the conduction band (usually in the range 0.2–0.4 eV above the ground state) by the light with a broad spectral range of energies. The electron falls down the conduction band very rapidly via cascadinglike emissions of the LO phonon, and finally drops into the energy region $\epsilon < \hbar\omega_{LO}$. The process of the cascading fall (with the emissions of 10–30 LO phonons) is believed to be accomplished within 1 psec.[56] The electron once dropping into the region $\epsilon < \hbar\omega_{LO}$, will be rapidly accelerated by E_x to reach the state $\epsilon = \hbar\omega_{LO}$, and thereafter it performs the streaming motion as described above. The streaming motion will continue until the electron is finally captured by shallow traps, where τ_t is several tens of psec as shown in Table I. The time T_{LO} was evaluated for AgCl and AgBr by using the values of m_p^* and $\hbar\omega_{LO}$ tabulated in Table II. The value of T_{LO} at $E_x = 1$ kV/cm is shown in Table III. T_{LO} at high electric fields is much shorter than τ_t. Second, we consider the effect of impurity scattering. In order that the streaming motion be realized in the experiment, the electron must be rapidly accelerated to $\epsilon = \hbar\omega_{LO}$ before being scattered by impurities; in other words, E_x must be intense enough such that $T_{LO} < \tau_{imp}$ is satisfied. In the present experiment, the minimum field E_m, at which $T_{LO} = \tau_{imp}$ holds, ranges from 100 to 1000 V/cm according to the purity of crystals used. The value of E_m evaluated for each crystal is indicated by an arrow on each curve in Figs. 7–10.[57] The streaming motion is considered possible for higher electric fields $E_x > E_m$.

We now examine the data of μ_H and v_d on the

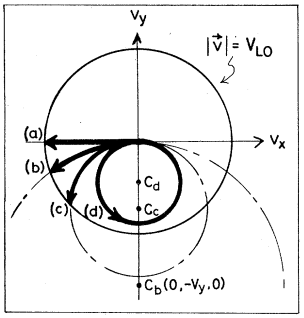

FIG. 21. Electron trajectories in the velocity space at $\vec{E} = (E_x, 0, 0)$ and $\vec{H} = (0, 0, H_z)$. (a) At $\zeta = 0$, the trajectory forms a straight line between the points $\vec{v} = 0$ and $\vec{v} = (-V_{LO}, 0, 0)$. (b) When $\zeta < 1$, the trajectory is curved forming a part of an arc around $C(0, -V_y, 0)$, where the point C is located outside of the circle $|\vec{v}| = V_{LO}$. (c) When $1 < \zeta < 2$, the center of the arc C enters the circle. (d) When $2 < \zeta$, the trajectory does not cross the circle $|\vec{v}| = V_{LO}$ and it forms a cyclotron full orbit within the circle.

scheme of streaming motion. The mean free time of an electron is given by $\frac{1}{2}T_{LO}$ when the electron is streaming. (Note that the time interval of successive emissions of the LO phonon is given by T_{LO}.) Therefore, we can get, most simply, the Hall mobility of a streaming electron in the form[58]

$$\mu_H^s = (e/m^*)(\tfrac{1}{2}T_{LO}), \tag{17}$$

by replacing τ in Eq. (11) by $\frac{1}{2}T_{LO}$. The quantity μ_H^s was evaluated as a function of E_x. The result is shown by a solid line in Fig. 7 and in the inset. We can note[59] that every curve of μ_H vs E_x begins to fall steeply just above the indicated field E_m and that all the data points at the higher E_x fall close to the solid line μ_H^s. These results definitely support the picture of streaming motion at high electric fields. The drift velocity of a streaming electron is given by a constant value $\frac{1}{2}V_{LO}$ independently of E_x;

$$v_d^s = \tfrac{1}{2}V_{LO}\,. \tag{18}$$

In every crystal, the drift velocity of electrons v_d is saturated to a value close to $\frac{1}{2}V_{LO}$ at high E_x above E_m as seen in Figs. 8–10. One can notice that the saturated value of v_d in Figs. 8–10 is slightly lower than the value $\frac{1}{2}V_{LO}$. In considering the discrepancy we should recall that v_d was estimated from the value of μ_H by assuming the relation $v_d = \mu_H E_x$(for AgCl *M*0-1 and AgBr *ZR*3-2 with $p=0$) and $v_d = 0.85\mu_H E_x$(for AgCl *M*1*CB* with $p=-\frac{1}{2}$). These relations are not generally correct when the electrons depart from the thermal equilibrium state. We will show in the Appendix that $v_d = \frac{3}{2}\mu_H E_x$ holds when the electron is streaming [see (A12)]. When we adopt the relation $v_d = \frac{3}{2}\mu_H E_x$ to estimate v_d, the agreement of the saturated drift velocity with $\frac{1}{2}V_{LO}$ becomes more satisfactory, but the saturated value of v_d slightly exceeds the value $\frac{1}{2}V_{LO}$ by a factor (5–10%).[60] The fact that v_d exceeds $\frac{1}{2}V_{LO}$ may reflect that the electron slightly intrudes into the higher energy range $\epsilon > \hbar\omega_{LO}$.[61]

C. Variation in the electron kinetics with E_x and H_z

Suppose that an electron is streaming at an intense electric field E_x in the absence of magnetic field [as described in Fig. 21(a)]. The theme in this section is to elucidate how the mode of the electron motion varies on application of a transverse magnetic field H_z. When H_z is applied, the trajectory of streaming electrons will be curved due to the Lorentz force as described by Figs. 21(b) and 21(c). It is shown in the Appendix that the curved trajectory at a given E_x and H_z is expressed by an arc on the $v_z = 0$ plane whose center is located at the point $C(0, -V_y, 0)$, where V_y has been defined by Eq. (13). The electron will repeatedly move on the arc from the point $\vec{v}=0$ to a point of the intersection of the trajectory with the surface $|\vec{v}| = V_{LO}$. In this case, the trajectory of streaming motion in the velocity space is determined by the relative position of the point C against the surface $|\vec{v}| = V_{LO}$. This means that the trajectory is specified by using the normalized field $\zeta \equiv V_{LO}(cE_x/H_z)^{-1}$. When $\zeta = 0$ ($H_z = 0$), the point C is located at $(0, -\infty, 0)$ and the trajectory is given by a straight line [Fig. 21(a)]. The point C is located outside the surface $|\vec{v}| = V_{LO}$ when $0 < \zeta < 1$ [Fig. 21(b)] and the point C enters the surface when $\zeta > 1$ [Fig. 21(c)]. At $\zeta = 2$, the trajectory skims the surface $|\vec{v}| = V_{LO}$ and the streaming motion of electrons becomes impossible for $\zeta > 2$ [Fig. 21(d)]. Several characteristic quantities of the streaming motion were calculated as a function of ζ for the range $\zeta < 2$. The results are summarized as follows.[62] The process of calculation is briefly shown in the Appendix.

First, the tangent of the Hall angle of the circular motion, $\tan\theta^s \equiv v_y^s/v_x^s$ (where v_x^s and v_y^s are the drift velocity of the streaming electron along the x and y direction, respectively), is expressed in the form, (A8);

$$\tan\theta^s = 2\zeta^{-2}\cos^{-1}(1-\tfrac{1}{2}\zeta^2) - (4\zeta^{-2}-1)^{1/2}\,. \tag{19}$$

Second, the time required for the electron to pass from the point $\vec{v}=0$ to the surface $|\vec{v}| = V_{LO}$ on the trajectory of streaming motion, $T_{LO}(E_x, H_z)$, has the expression, (A5),

$$T_{LO}(E_x, H_z) = T_{LO}\zeta^{-1}\cos^{-1}(1-\tfrac{1}{2}\zeta^2)\,, \tag{20}$$

where T_{LO} in the right-hand side of the equation is defined by Eq. (16). Third, the magnitude of the drift velocity in the $x-y$ plane, $v_{xy}^s \equiv [(v_x^s)^2 + (v_y^s)^2]^{1/2}$, is obtained in the form, (A9),

$$v_{xy}^s = V_{LO}[\zeta\cos^{-1}(1-\tfrac{1}{2}\zeta^2)]^{-1} \times \{\tfrac{1}{4}\zeta^4 + [\cos^{-1}(1-\tfrac{1}{2}\zeta^2) - (\zeta^2 - \tfrac{1}{4}\zeta^4)^{1/2}]^2\}^{1/2}\,. \tag{21}$$

We evaluated these quantities by using the values of the cold polaron mass m_p^* and $\hbar\omega_{LO}$ for AgCl and AgBr (Table II). Let us compare these results with the present data of $\tan\theta$, Q_z, and $(Q_x^2+Q_y^2)^{1/2}$.

1. In the range $\zeta < 1$ (circular streaming)

Equation (19) is shown by a solid line as a function of ζ for AgCl in Fig. 16 and for AgBr in the inset. It should be emphasized that no fitting parameters are involved in the comparison of Eq. (19) with the data of $\tan\theta$. In the range $\zeta < 1$, agreement of the data points with the calculated value is satisfactory. This assures us that the picture of circular streaming [Fig. 21(b)] gives a proper description of the phenomena in this

range. Still, the measured value of $\tan\theta$ is slightly higher than the calculated one [by a factor (5–15%) for AgCl] in this range. This may indicate that the electron slightly intrudes into the higher energy range $\epsilon > \hbar\omega_{LO}$. Let us further consider the case when a weak electric field E_z is also applied on the electron to interprete the result of Q_z. The field E_z accelerates the electron towards the z direction with the acceleration rate $-eE_z/m^*$ and the time of acceleration is limited to $T_{LO}(E_x, H_z)$ by successive emissions of the LO phonon. Therefore, the electron will acquire the drift velocity along the z direction of the magnitude of

$$v_z^s = -(e/m^*)(\tfrac{1}{2}T_{LO})E_z , \tag{22}$$

where T_{LO} is given by Eq. (20). In the Q_z measurements (in Figs. 19 and 20), overall decreases in the current Q_z are observed with increasing E_x. These phenomena indicate that $T_{LO}(E_x, H_z)$ decreases with increasing E_x. In other words, the successive emissions of the LO phonon become more and more frequent as E_x increases and this gives rise to an overall decrease of Q_z with E_x. In order to quantitatively compare Eq. (20) with the data of Q_z, let us recall that the data points of Q_z in Fig. 19 represent the quantity $[\tau_t(E_x, H_z)/\tau_t(0,0)]v_z$. The quantity $\tau_t(E_x, H_z)/\tau_t(0,0)$ itself is so far an unknown function of E_x and H_z but the value $\tau_t(E_x, 0)/\tau_t(0,0)$ is known as a function of E_x from the data of $Q_x(E_x)$ and $v_d(E_x)$ shown in Fig. 9. Here let us introduce the following quantity on the assumption that $\tau_t(E_x, H_z)$ is independent of H_z,

$$Q_z^{cal}(E_x, H_z) \equiv [\tau_t(E_x, 0)/\tau_t(0,0)]v_z^s , \tag{23}$$

where v_z^s is given by Eq. (22). Solid lines (a), (b), and (c) in Fig. 19 are drawn according to Eq. (23) for $E_x = 1200$, 2400, and 3400 V/cm respectively, where the quantity $\tau_t(E_x, 0)/\tau_t(0,0)$ was deduced from the data of Q_x and v_d shown in Fig. 9. As seen from Fig. 19, agreements between the lines (a)–(c) and the corresponding data points are almost perfect in the range $\zeta < 1$. (Also in this case, no arbitrary parameters are involved in the comparison.) This indicates that (i) Eq. (22) is valid and the streaming electron successively emit the LO-phonon with the time interval $T_{LO}(E_x, H_z)$ given by Eq. (20) in the range $\zeta < 1$ and (ii) the trapping lifetime $\tau_t(E_x, H_z)$ does not vary with H_z in the range $\zeta < 1$; $\tau_t(E_x, H_z) \cong \tau_t(E_x, 0)$ for $\zeta < 1$. Thus the experimental result of Q_z assures again the validity of the picture of streaming motion. We will discuss the behavior of the trapping lifetime further in detail in Sec. IV D.

2. *In the range $1 < \zeta < 2$ (circular streaming and population inversion)*

All the curves of $\tan\theta$ vs ζ begin to rise steeply and largely deviate from the calculated curve in the range $\zeta > 1$ (in Fig. 16 and in the inset). All the curves of Q_z vs H_z also begin to rise steeply giving a large deviation from the calculated curve in the range $\zeta > 1$ (in Fig. 19). Thus the simple picture of the streaming motion fails to explain the data of $\tan\theta$ and Q_z in the range $\zeta > 1$. Hence, we derive the following scheme of the electron distribution, with a help of Maeda and Kurosawa's prediction.[6] In the range $\zeta > 1$, the point C enters the surface $|\vec{v}| = V_{LO}$ and consequently there emerges a spindle shape region K in which the trajectory of electrons does not cross the surface $|\vec{v}| = V_{LO}$ [see Fig. 22(c)]. If an electron jumps into the area via some scattering mechanism, it will stay within this area for a long time without being removed from this area. (The electron in K never reaches the state $|\vec{v}| = V_{LO}$ and is able to continue its cyclotron oscillation until it is scattered by impurities.) This situation should be compared with that for electrons at the rest of the area: An electron at any state outside of the area K will be rapidly accelerated to the state $|\vec{v}| = V_{LO}$ and scattered to the ground state $\vec{v} = 0$. With this sit-

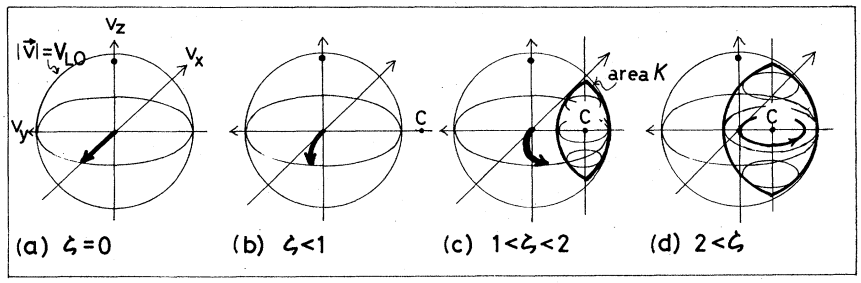

FIG. 22. Variation in the hot electron distribution with ζ. (a) All the electrons distribute on the trajectory of streaming. (b) Trajectory is curved around the point $C(0, -V_y, 0)$. (c) Some of electrons accumulate into a spindle shape area K, while the other electrons still distribute on the trajectory of streaming. (d) Trajectory for streaming disappears and all the electrons are on cyclotron orbits within the area K.

uation it is possible that a certain amount of electrons accumulate within the area K, provided a suitable mechanism of electron scattering is able to supply electrons to the area K. (Vosilius and Levinson[5] first noted the existence of the area K, and subsequently, Maeda and Kurosawa[6] pointed out the possibility of electron accumulation into the area K on the basis of a Monte Carlo calculation on p-type Ge.) The mechanism for the accumulation will be discussed later. If a certain amount of electrons accumulate in the area K, the electrons in K make a large contribution to the Hall current but little to the current Q_x. Therefore, the Hall angle of a superposed current must yield higher value than that of the calculated one deduced only for the group of streaming electrons. This explains the observed behavior of $\tan\theta$ very well.[18,20] The scatter of the data points of $\tan\theta$ in the range $\zeta > 1$ then indicates that the amount of those electrons accumulated in the area K depends on the purity of specimens and the strength of applied electric field E_x, as will be numerically analyzed later. In the case that E_z is applied, the electrons in K will yield a larger current Q_z [than Q_z^{cal} given in Eq. (23)] since they have a long scattering time as compared with the streaming electrons.[19,20] Thus, both behavior of $\tan\theta$ and of Q_z in the range $\zeta > 1$ provide definite evidence for the electron accumulation in the area K. The electron distribution in the range $1 < \zeta < 2$ is believed to consist of two groups of electrons: A certain amount of electrons are accumulated in the area K, whereas the rest of the electrons are streaming, as described in Fig. 22(c).

One can note in the inset of Fig. 16 that the curves of $\tan\theta$ vs ζ for AgBr bend over in the range $\zeta^h > 1$. This indicates that in AgBr positive holes also accumulate into the area K in the range $\zeta^h > 1$. The impurity scattering time of holes in AgBr $ZR3$-2 is as long as 13 psec (Table I), which should be compared with the value $T_{\mathrm{LO}}^h = 4.2$ psec at $E_x = 1$ kV/cm (Table III). Thus it is not surprising that the holes are streaming at high E_x in the range $\zeta^h < 1$ and accumulate into the area K in the range $\zeta^h > 1$. The feature of $\tan\theta$-ζ curve is simple for AgCl, giving no indication for the conduction of positive holes.

Let us consider the mechanism of accumulation. The electrons in K have a finite lifetime; the electrons will be scattered out of the area K via the impurity scattering. Therefore, there must exist a suitable mechanism to supply electrons into the area K, in order that a certain amount of electrons accumulate within the area K. First, impurities may scatter electrons from the trajectory of streaming into the area K. Nevertheless this cannot be the mechanism since the same process also removes electrons out of the area K. Second, it may happen that an electron, which is initially photoexited at a high energy state in the conduction band, drops into the area K after a cascadinglike emission of LO phonons. This process is not likely to produce a sufficient amount of accumulation to explain the observed behavior of $\tan\theta$ and Q_z. (The "volume of the area K", V_K, is a small fraction of the "total volume" of the sphere $|\vec{v}| \leqq V_{\mathrm{LO}}, V_{\mathrm{tot}}$. For example, $V_K/V_{\mathrm{tot}} \sim 0.05$ at $\zeta = 1.4$, whereas the ratio of the number of accumulated electrons in K to that of the streaming electrons reaches about 0.15 as will be seen in Fig. 23.) This mechanism neither explains the scatter of the data points of $\tan\theta$ in the range $\zeta > 1$. Finally, the most likely mechanism, suggested by Kurosawa, is described as follows. A streaming electron may happen to reach a higher-energy state, $\epsilon = \hbar\omega_{\mathrm{LO}} + \Delta\epsilon$, and to jump into the area K with an excess energy $\epsilon = \Delta\epsilon$ after the LO-phonon emission. Although the probability of such a process may be low, the electron accumulation may be realized via this mechanism since (i) the streaming electron very frequently repeats the LO-phonon emission and (ii) the electron once jumping into the area K stays in this area for a long time. Let us treat this mechanism quantitatively by assuming that n_s electrons are streaming, n_K electrons are in K and the probability of a streaming electron jumping into the area K after the LO phonon emission is γ. Then, the number of those electrons jumping into and going out of the area K per unit time is given, respectively, by $n_s\gamma/T_{\mathrm{LO}}$ and $n_K/\tau^K{}_{\mathrm{imp}}$, where T_{LO} is defined by Eq. (20) and $\tau^K{}_{\mathrm{imp}}$ denotes the impurity scattering time of electrons in the area K. From the balance equation,

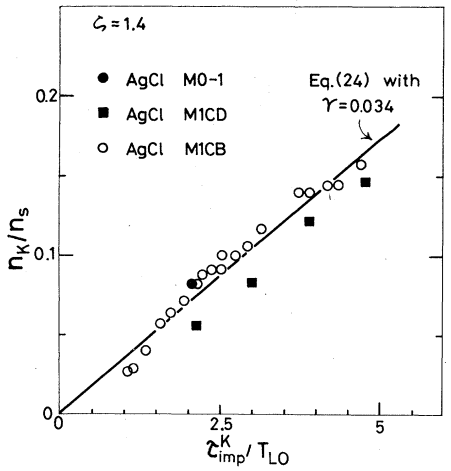

FIG. 23. Ratio in number of the electrons in the area K to the electrons in streaming at $\zeta = 1.4$. The ratio n_K/n_s is plotted as a function of $\tau^K_{\mathrm{imp}}/T_{\mathrm{LO}}$.

we obtain the ratio[63] of n_K to n_s;

$$n_K/n_s=\gamma(\tau^K{}_{\rm imp}/T_{\rm LO})\,. \tag{24}$$

One can note the following points in the feature of $\tan\theta$-ζ curves in the range $\zeta>1$ (Fig. 16). (a) For each crystal, the rise of the curve with ζ is steeper for higher E_x. (b) The rise is steeper for the crystal of longer $\tau^0{}_{\rm imp}$. [For example, compare the curve for AgCl $M0$-1 crystal ($\tau^0{}_{\rm imp}=6.9$ psec and $p=0$) at 3700 V/cm with that for the $M1CD$ crystal ($\tau^0{}_{\rm imp}=3.7$ psec and $p=0$) at 4070 V/cm.] (c) The rise is steeper for a crystal of $p=0$ than for a crystal of $p=-\frac{1}{2}$. [For example, compare the curve for the $M0$-1 crystal ($\tau^0{}_{\rm imp}=6.9$ psec and $p=0$) at 1800 V/cm with that for the $M1CB$ crystal ($\tau^0{}_{\rm imp}=9.5$ psec and $p=-\frac{1}{2}$) at 3300 V/cm.] These observations are interpreted in terms of Eq. (24), which insists that the accumulation should be enhanced with longer $\tau^K{}_{\rm imp}$ and the higher value of E_x. ($T_{\rm LO}^{-1}$ is proportional to E_x at a fixed value of ζ. Note also that $\tau^K{}_{\rm imp}=\tau^0{}_{\rm imp}$ for a crystal of $p=0$ but $\tau^K{}_{\rm imp}<\tau^0{}_{\rm imp}$ for a crystal of $p=-\frac{1}{2}$ since the area K is located at a high-energy region within the surface $|\vec{v}|=V_{\rm LO}$.) We have estimated the value of n_K/n_s from the data of $\tan\theta$ and checked the validity of Eq. (24). The superposed current of the two groups of electrons will have the Hall angle of the form

$$\tan\theta=(n_s v_y^s+n_K v_y^K)/(n_s v_x^s+n_K v_x^K)\,,$$

where $v^s{}_{x,y}$ represents the drift velocity of a streaming electron in the x and y direction, and $v^K{}_{x,y}$ is the averaged drift velocity of electrons in K in the x and y direction. v_x^s and v_y^s are given by Eqs. (A6) and (A7). By setting $v_x^K=0$ and $v_y^K=-V_y$, we obtain the form

$$\tan\theta=\tan\theta^s-(n_K/n_s)(V_y/v_x^s)\,, \tag{25}$$

where $\tan\theta^s\equiv v_y^s/v_x^s$ is given by Eq. (19). Using Eq. (25), we can estimate the value of n_K/n_s from the observed magnitude of $\tan\theta$ at a given ζ.[64] The quantity n_K/n_s at $\zeta=1.4$ in three different AgCl crystals is plotted together as a function of $\tau^K{}_{\rm imp}/T_{\rm LO}$ in Fig. 23. [$\tau^K{}_{\rm imp}$ for $M1CB$ at $\zeta=1.4$ was calculated by the relation $\tau^K{}_{\rm imp}=\tau^0{}_{\rm imp}(\epsilon/kT)^{-1/2}$, where ϵ is set to be $(m^*/2)(V_{\rm LO}/1.4)^2$; the energy value of the point $C(0,-V_y,0)$ for $\zeta=1.4$.] Data points of the estimated value of $(n_K/n_s)_{\zeta=1.4}$ fall close to a solid line drawn according to Eq. (24) with the constant $\gamma=0.034$.

3. In the range $\zeta>2$ (stable cyclotron motion in the region K)

In the range $\zeta>2$, the trajectory for streaming disappears as shown in Fig. 21(d) and all the electrons will therefore distribute on the cyclotron orbits within the area K [see Fig. 22(d)]. The averaged drift velocity of electrons will then be $\sim(0,-V_y,0)$. The data of Q_x, Q_y, and $\tan\theta$ are consistent with this picture. The current Q_x falls down to a small level at $\zeta=2$ as seen in Fig. 11. The small current Q_x remaining in the range $\zeta>2$ comes from the residual impurity scattering. The tangent of the Hall angle goes up to have a high value at $\zeta=2$ (Figs. 15 and 16). Solid lines in Fig. 12 indicate the velocity V_y as a function of H_z for $E_x=920$, 1850 and 3700 V/cm. The velocity V_y is also shown as a function of E_x for $H_z=32$ and 57.6 kOe in the inset of Fig. 12. One can notice that the data points of Q_y fall close to the solid lines indicating V_y in the range $\zeta>2$. This indicates that the speed of electrons in the y direction is V_y in the range $\zeta>2$. From the fact that Q_y fall close to the solid lines V_y, we should also notice that the trapping lifetime of electrons is reduced to the low-field value in the high-magnetic-field range; $\tau_t(E_x,H_z)\sim\tau_t(0,0)$ in the range $\zeta>2$.

Thus, we have succeeded in explaining the phenomena on a basis of the classical picture. It is well known in quantum mechanics that the motion of a free electron at crossed fields is quantized into the Landau state.[65] The Landau quantization is insignificant for streaming electrons since the frequent phonon emission breaks the scheme of quantization. On the other hand, the quantization effect may be significant for electrons in the area K since those electrons have long scattering time. Then we should expect a set of "Landau cylinders" within the area K. Such a quantized structure within the area K, however, was not noted in the present experiment, in which the Landau splitting $\hbar\omega_c$ is believed not large enough compared to $\hbar\omega_{\rm LO}$. (The value of $\hbar\omega_c$ in AgCl is only about one sixteenth of $\hbar\omega_{\rm LO}$ even at 60 kOe.)

D. Variation in the trapping lifetime of electrons with E_x and H_z

Photoelectrons in AgCl and AgBr crystals at helium temperatures are captured by shallow trap centers. Heyningen and Brown[66] and Brandt and Brown[67] investigated the nature of shallow traps which dominate the electron capture at helium temperatures in pure AgBr and AgCl crystals. The ground state of the trap centers has been estimated to lie 36.2 (AgCl) and 23.8 meV (AgBr) below the bottom of the conduction band. Sakuragi *et al.*[68] supposed the trap centers to be interstitial Ag^+ ion for both AgCl and AgBr crystals. The electron once captured by the trap centers can never be thermally excited to the conduction band

in the time of photocurrent measurements at 4.2 K.[69] The trapping lifetime τ_t in the crystals presently used has a value ranging from 10 to 100 psec at low electric fields (Table I).

We have pointed out in Sec. III B that the trapping lifetime $\tau_t(E_x, H_z)$ at $H_z = 0$ increases with E_x. We have also mentioned about the behavior of τ_t against H_z (in Secs. IV C 1 and IV C 3). One can clearly see from Fig. 18 how $\tau_t(E_x, H_z)$ varies with H_z. The magnitude of the drift velocity, $v_{xy}(E_x, H_z)$, is expected to be v_{xy}^s [given by Eq. (21)] in the range $\zeta < 1$ and to be V_y ($= V_{LO}\zeta^{-1}$) in the range $\zeta > 2$. A solid line in Fig. 18 represents v_{xy}^s as a function of ζ in the range $\zeta < 2$ and represents V_y in the range $\zeta > 2$. We should note that each $Q_{xy} - \zeta$ curve at high E_x is almost parallel with the solid line in the range $\zeta < 1$. This means that the increased trapping lifetime stands almost constant against H_z in the range $\zeta < 1$; $\tau_t(E_x, H_z) \cong \tau_t(E_x, 0)$. This behavior of τ_t has also been suggested from the independent data of Q_z in Sec. IV C 1. Next, we should note that all the data points of Q_{xy} begin to fall at $\zeta = 1$ and converge to the solid line in the range $\zeta > 2$. This indicates that τ_t begins to decrease with H_z above $\zeta = 1$ and is reduced to the low-field lifetime in the range $\zeta > 2$; $\tau_t(E_x, H_z) \cong \tau_t(0, 0)$ for $\zeta > 2$. This has been suggested from the Q_y data in Sec. IV C 3.

We can summarize the behavior of $\tau_t(E_x, H_z)$ at high electric fields as follows:

(i) At $H_z = 0 (\zeta = 0)$, τ_t increases with E_x; $\tau_t(E_x, 0) > \tau_t(0, 0)$. The strength of electric field at which τ_t begins to increase depends on the sample. In each sample, the increase in τ_t coincides with the saturation in v_d.

(ii) In the range $\zeta < 1$, τ_t increases with E_x whereas it is almost independent of H_z; $\tau_t(E_x, H_z) \cong \tau_t(E_x, 0)$.

(iii) In the range $1 < \zeta < 2$, τ_t decreases with H_z.

(iv) In the range $\zeta > 2$, τ_t is almost identical to the low-field value; $\tau_t(E_x, H_z) \cong \tau_t(0, 0)$.

Thus, the behavior of τ_t is characterized again by the quantity ζ. Let us consider the physical mechanism for the variation in τ_t. First, the capture rate of electron by traps may depend on the electron energy. This is not likely the mechanism for the present case, since the variation in τ_t is observed in the range of E_x and H_z where the average energy of electrons is believed to be almost constant. Second, the electric field applied may distort the wave function of trapped states of electrons giving rise to a variation in the capture rate. One cannot explain (i) the sample dependence in the increase in τ_t with E_x in terms of this effect. It is also hard to explain (ii) the magnetic field dependence of τ_t in terms of this effect. We should note the following points. (a) The increase in τ_t coincides with the occurrence of the streaming motion. (b) The increased lifetime τ_t is kept unchanged where all the electrons are streaming. (c) The increased lifetime begins to decrease where the accumulation sets in and the number of streaming electrons decreases. (d) The lifetime is reduced to the low-field lifetime where the streaming motion disappears. All these points strongly suggest that the streaming motion is responsible for the increase in τ_t. It is hard, however, to explain the variation in the capture rate of electrons by the simple classical picture of the streaming motion. The behavior described above of τ_t appears to give us an open problem for the polaron capture process. It appears that a possible correlation between successive emissions of the LO phonon by a polaron reduces the capture rate of the polaron by traps. It should also be considered that the streaming motion may affect the "polaron self-energy."

V. CONCLUSION

Galvanomagnetic effects of hot electrons in zone-refined AgCl and AgBr crystals have been investigated at 4.2 K in crossed electric field E_x up to 5 kV/cm and magnetic field up to 58 kOe. It was found that the LO-phonon emission by electrons dominates all the other scattering mechanisms at high E_x. The drift velocity of electrons is saturated to the value $\frac{1}{2} V_{LO}$ at high electric fields, where $\frac{1}{2} m^* V_{LO}^2 \equiv \hbar\omega_{LO}$. All the electrons are believed to distribute on the streaming trajectory which forms, in the velocity space, a line between the two points $\vec{v} = 0$ and $\vec{v} = (-V_{LO}, 0, 0)$. The effect of applying transverse magnetic fields H_z on streaming electrons is described in terms of a normalized field $\zeta \equiv V_{LO}/V_y = (2\hbar\omega_{LO}/m^*)^{1/2} (cE_x/H_z)^{-1}$, where $V_{LO} \equiv (2\hbar\omega_{LO}/m^*)^{1/2}$ and $V_y \equiv cE_x/H_z$. First, in a relatively low H_z range (; relatively high E_x range), $\zeta < 1$, the only effect of H_z is to bend the trajectory of streaming towards the y direction. Accordingly, the Hall current Q_y emerges and the tangent of the Hall angle, $\tan\theta \equiv Q_y/Q_x$, increases with ζ. The magnitude of the current $Q_{xy} \equiv (Q_x^2 + Q_y^2)^{1/2}$ remains almost unchanged in this range. The observed value of $\tan\theta$ in this range is quantitatively interpreted in terms of the picture of streaming motion. All the electrons are believed to distribute on an arc trajectory passing the point $\vec{v} = 0$ with the center at the point $C \equiv (0, -V_y, 0)$. The probe current Q_z, which is the response to a weak electric field E_z, gives an evidence that the mean free time of the streaming electron is limited by successive emissions of the LO phonon. Secondly, in

an intermediate range $1<\zeta<2$, the point C enters the surface $|\vec{v}| = V_{LO}$ and there appears a new group of electrons (n_K) accumulated in a high energy area K, while the other electrons (n_s) are still distributed on the arc trajectory of streaming. According to this population inversion, drastic changes take place in Q_x, Q_y and also in Q_z; namely, $\tan\theta$ and Q_z abruptly increase and Q_{xy} decreases with increasing ζ in the range $1<\zeta<2$. These observations provide a first experimental evidence for the population inversion of the type as has been predicted by Maeda and Kurosawa.[6] The ratio of the population inversion n_K/n_s is noted to be an increasing function of E_x and of the impurity scattering time. Finally, in a relatively high-magnetic-field range (relatively low-electric-field range), $\zeta>2$, the streaming trajectory disappears and accordingly all the electrons are obliged to distribute on the cyclotron full orbits around the point C. It is directly confirmed from the data of Q_y that the drift velocity of electrons in the y direction is $-V_y$ in the range $\zeta>2$. Some experimental evidence for the analogous behavior of positive holes in AgBr crystals is also presented.

The trapping lifetime of electrons $\tau_t(E_x, 0)$ increases with E_x in the high electric field range where the streaming motion is realized; $\tau_t(E_x, 0) > \tau_t(0, 0)$; where $\tau_t(0, 0)$ is the lifetime at low electric and magnetic fields. It is found that the application of high magnetic field H_z reduces the (increased) lifetime $\tau_t(E_x, 0)$ to a low-electric-field value $\tau_t(0, 0)$; namely, $\tau_t(E_x, H_z) = \tau_t(0, 0)$ for $\zeta>2$. It is suggested that the streaming motion of an electron (or successive emissions of the LO phonon) plays an essential role in giving rise to a variation in τ_t.

Thus, conclusive evidence was experimentally obtained, for the first time, for the streaming motion, the anomalous distribution, and the population inversion of electrons and holes in AgCl and AgBr crystals at 4.2 K in crossed electric and magnetic fields.

ACKNOWLEDGMENTS

The authors are grateful to Professor T. Kurosawa for valuable discussions and to Professor W. Sasaki and Dr. J. W. Hodby for critical readings of the manuscript. They thank Dr. F. Moser and A. Muramatsu for providing them with the samples. This work was supported by the Grants-in-Aid for Scientific Research (A) and for Special Project Research, both from the Ministry of Education, Science, and Culture.

APPENDIX: STREAMING MOTION OF ELECTRONS IN E_x AND H_z

The equation of motion of a free electron in an electric field $\vec{E}$ and a magnetic field $\vec{H}$ is given in the form

$$m^* \frac{d}{dt}\vec{v}(t) = -e\vec{E} - \frac{e}{c}(\vec{v}(t)\times\vec{H}). \tag{A1}$$

For $\vec{E} = (E_x, 0, 0)$ and $\vec{H} = (0, 0, H_z)$, this equation has the next solution under the initial condition $\vec{v}(0) = 0$,

$$v_x(t) = -V_y \sin\omega_c t, \tag{A2}$$

$$v_y(t) = V_y(\cos\omega_c t - 1), \tag{A3}$$

and

$$v_z(t) = 0, \tag{A4}$$

with $V_y \equiv cE_x/H_z$ and $\omega_c \equiv eH_z/m^*c$. Equations (A2)–(A4) represent the cyclotron motion of an electron in the velocity space. The center of the cyclotron orbit is the point $C \equiv (0, -V_y, 0)$; namely, the electron drifts along the y direction with the velocity $-V_y$. Here, we suppose that an electron which reaches the surface $|\vec{v}| = V_{LO}$ is immediately scattered back to the ground state $\vec{v} = 0$. Then the trajectory of streaming motion forms a part of the cyclotron orbit as illustrated in Fig. 21. When $\zeta \equiv V_{LO}/V_y > 2$, the full orbit of the cyclotron motion is closed within the surface $|\vec{v}| = V_{LO}$ as illustrated in Fig. 21(d). In the following, we only consider the case $\zeta<2$. Let us denote by $T_{LO}(E_x, H_z)$ the time required for an electron to pass from the point $\vec{v} = 0$ to the surface $|\vec{v}| = V_{LO}$ at E_x and H_z. The time $T_{LO}(E_x, H_z)$ is obtained from the equation, $[v_x^2(t) + v_y^2(t)]^{1/2} = V_{LO}$. Using Eqs. (A2) and (A3), we obtain

$$T_{LO} = [(2m^*\hbar\omega_{LO})^{1/2}/eE_x]\,\zeta^{-1}\cos^{-1}(1 - \tfrac{1}{2}\zeta^2), \tag{A5}$$

The drift velocities of the streaming electron along the x and y directions are obtained by averaging $v_x(t)$ and $v_y(t)$ over the time; namely,

$$v_x^s = (T_{LO})^{-1}\int_0^{T_{LO}} v_x(t)\,dt$$

and

$$v_y^s = (T_{LO})^{-1}\int_0^{T_{LO}} v_y(t)\,dt.$$

Elementary calculations of the integrals give

$$v_x^s = -V_y[(1 - \cos\omega_c T_{LO})/\omega_c T_{LO}] \tag{A6}$$

and

$$v_y^s = -V_y[(\omega_c T_{LO} - \sin\omega_c T_{LO})/\omega_c T_{LO}]. \tag{A7}$$

We obtain the tangent of the Hall angle of the streaming motion $\tan\theta^s = v_y^s/v_x^s$ from Eqs. (A5)–(A7) in the form

$$\tan\theta^s = 2\zeta^{-2}\cos^{-1}(1-\tfrac{1}{2}\zeta^2) - (4\zeta^{-2}-1)^{1/2}. \quad \text{(A8)}$$

We define v_{xy}^s, the magnitude of the drift velocity on the x-y plane, by the equation $v_{xy}^s = [(v_x^s)^2 + (v_y^s)^2]^{1/2}$ with v_x^s and v_y^s given by (A6) and (A7). Using (A5), we obtain v_{xy}^s directly from (A6) and (A7) in the form

$$v_{xy}^s = V_{\mathrm{LO}}[\zeta\cos^{-1}(1-\tfrac{1}{2}\zeta^2)]^{-1} \times\{\tfrac{1}{4}\zeta^4 + [\cos^{-1}(1-\tfrac{1}{2}\zeta^2) - (\zeta^2-\tfrac{1}{4}\zeta^4)^{1/2}]^2\}^{1/2}. \quad \text{(A9)}$$

To meet the previous definition of the Hall mobility [Eq. (9)], we define the Hall mobility of the streaming electron by

$$\mu_H^s \equiv \lim\left(\frac{c}{H_z}\left|\frac{v_y^s}{v_x^s}\right|\right).$$

By developing the trigonometrical function in Eqs. (A6) and (A7) into series, we obtain μ_H^s in the form

$$\mu_H^s = (e/m^*)(\tfrac{1}{3}T_{\mathrm{LO}}). \quad \text{(A10)}$$

The drift velocity of a streaming electron at $H_z = 0$ is

$$v_d^s = \lim_{\omega_c\to 0} v_x^s = \tfrac{1}{2}V_{\mathrm{LO}} = (e/m^*)(\tfrac{1}{2}T_{\mathrm{LO}})E_x. \quad \text{(A11)}$$

Thus the relation between v_d^s and μ_H^s is

$$v_d^s = \tfrac{3}{2}\mu_H^s E_x. \quad \text{(A12)}$$

So far, we have adopted the condition $\vec{v}(0)=0$ for the initial velocity. Under an arbitrary initial velocity $\vec{v}(0) = (v_x^0, v_y^0, v_z^0)$, Eq. (A1) has the following solution:

$$v_x(t) = -V\sin(\omega_c t + \Theta), \quad \text{(A13)}$$

$$v_y(t) = V\cos(\omega_c t + \Theta) - V_y, \quad \text{(A14)}$$

and

$$v_z(t) = v_z^0, \quad \text{(A15)}$$

where V and Θ are determined by the initial velocity

$$-V\sin\Theta = v_x^0 \quad \text{(A16)}$$

and

$$V\cos\Theta - V_y = v_y^0. \quad \text{(A17)}$$

The kinetic energy of an electron oscillates with time. The maximum energy exceeds $\hbar\omega_{\mathrm{LO}}$ irrespective of the choice of initial velocity when $\zeta<1$. For $1<\zeta<2$, on the other hand, it is possible that the energy of electron never reaches $\hbar\omega_{\mathrm{LO}}$ when the initial velocity satisfies the relation

$$(V+V_y)^2 + (v_z^0)^2 < V_{\mathrm{LO}}^2. \quad \text{(A18)}$$

Electrons with the initial velocities satisfying (A18) have long scattering time against the phonon emission. The group of the trajectories of such electrons forms the spindle-shaped region K as shown in Fig. 22(c).

---

*Based on a thesis submitted by Susumu Komiyama in the fulfillment of requirements for the D.Sc. degree at the University of Tokyo, March 1976.

†Present address: Institut für Angewandte Physik, Universität Hamburg, 2 Hamburg 36, Jungiusstrasse 11, Federal Republic of Germany.

[1]W. Shockley, Bell Syst. Tech. J. 30, 990 (1951).

[2]See, for example, E. M. Conwell, Solid State Phys. Suppl. 9 (1967).

[3]T. Kurosawa and H. Maeda, J. Phys. Soc. Jpn. 31, 668 (1971).

[4]J. T. Devreese and R. Evrard, Phys. Status Solidi 78, 85 (1976).

[5]I. I. Vosilyus and I. B. Levinson, Zh. Eksp. Teor. Fiz. 50, 1660 (1966) [Sov. Phys.–JETP 23, 1104 (1966)]; 52, 1013 (1967) [25, 672 (1967)].

[6]H. Maeda and T. Kurosawa, in *Proceedings of the Eleventh International Conference on the Physics of Semiconductors, Warsaw, 1972* (Elsevier, New York, 1972), p. 602.

[7]Experimentally, W. E. Pinson and R. Bray [Phys. Rev. 136, A1449 (1964)] have first observed a large deviation of the hot electron distribution function from the Maxwellian type in p-type Ge at 77 K. They suggested the streaming motion of carriers in p-type Ge at high electric fields in the absence of magnetic field. As compared with their experiment, the present experiment has been made in an extreme condition; the lattice temperature is much lower ($T=4.2$ K) and the interaction between carriers and the LO phonon is much stronger. An ideal streaming motion results from these conditions in the present work.

[8]T. Masumi, Phys. Rev. 159, 761 (1967).

[9]D. Matz and F. Garcia-Moliner, J. Phys. Chem. Solids 26, 551 (1965).

[10]K. Kajita and T. Masumi, in *Proceedings of the Twelfth International Conference on the Physics of Semiconductors, Stuttgart, 1974* (Teubner, Stuttgart, 1974), p. 844.

[11]F. Nakazawa and H. Kanzaki, J. Phys. Soc. Jpn. 20, 468 (1965).

[12]T. Kawai, K. Kobayashi, and H. Fujita, J. Phys. Soc. Jpn. 21, 453 (1966).

[13]M. Mikkor and F. C. Brown, Phys. Rev. 162, 841 (1967).

[14]S. B. Bolte and F. C. Brown, in *Proceedings of the*

Third International Conference on Photoconductivity, 1971 (Pergamon, New York, 1971), p. 139.
[15]S. Komiyama and T. Masumi, Solid State Commun. 26, 381 (1978).
[16]S. Komiyama and T. Masumi, in *Proceedings of the Fourteenth International Conference on Physics of Semiconductors, Edinburgh, 1978*, edited by B. L. H. Wilson (The Institute of Physics, Bristol, 1978), p. 335.
[17]S. Komiyama and T. Masumi, Proceedings of the International Conference on Solids and Plasmas in High Magnetic Fields, Cambridge, 1978, J. Magn. Magn. Mater. (to be published).
[18]S. Komiyama, T. Masumi, and K. Kajita, in *Proceedings of the Thirteenth International Conference on the Physics of Semiconductors, Roma, 1976* (Tipografia Marves, Roma, 1976), p. 1222.
[19]S. Komiyama, T. Masumi, and K. Kajita, Phys. Rev. Lett. 42, 600 (1979).
[20]S. Komiyama, T. Masumi, and K. Kajita, Solid State Commun. 31, 447 (1979).
[21]F. C. Brown, in *Polarons and Excitons*, edited by C. G. Kuper and G. D. Whitfield (Oliver and Boyd, London, 1963).
[22]B. L. Joesten and F. C. Brown, Phys. Rev. 148, 919 (1966).
[23]Band calculations have been done by A. B. Kunz, Phys. Status Solidi 29, 115 (1968); and by P. M. Scop, Phys. Rev. 139, A934 (1965).
[24]As an experimental support, see, for example, Refs. 36 and 28.
[25]H. Tamura, Solid State Commun. 10, 297 (1972).
[26]H. Hohne and M. Stasiw, Phys. Status Solidi 28, 247 (1968).
[27]H. Kanzaki, S. Sakuragi, and K. Sakamoto, Solid State Commun. 9, 999 (1971).
[28]H. Tamura and T. Masumi, Solid State Commun. 12, 1183 (1973).
[29]T. D. Lee, F. E. Low, and D. Pines, Phys. Rev. 90, 297 (1953).
[30]G. D. Whitfield and R. Puff, Phys. Rev. 139, A338 (1965).
[31]D. M. Larsen, Phys. Rev. 144, 697 (1966).
[32]We owe the numerical evaluation to H. Tamura.
[33]J. W. Hodby, J. G. Crowder, and C. C. Bradley, J. Phys. C 17, 3033 (1974).
[34]For example, J. W. Hodby, in *Polarons in Ionic Crystals and Polar Semiconductors*, edited by Devreese (American Elsevier, New York, 1972), p. 389. See also Ref. 21.
[35]D. C. Burnham, F. C. Brown, and R. S. Knox, Phys. Rev. 119, 1560 (1960).
[36]H. H. Tippins and F. C. Brown, Phys. Rev. 129, 2554 (1963).
[37]Y. Iye and K. Kajita, Solid State Commun. 17, 957 (1975).
[38]τ_t was roughly estimated from the magnitude of photocurrent by taking into account the intensity of excitation light. (The quantum yield was assumed to be 1.) For the AgBr *ZR*3-2 crystal, τ_t was estimated more accurately, the procedure of which will be described in Sec. III B.
[39]S. Komiyama, D. Sc. thesis (Tokyo University, 1976) (unpublished). We can show that Eqs. (1) and (2) strictly hold on the assumption that (a) the electrodes and the specimen are perfectly symmetric and (b) carriers are generated symmetrically along the y direction. In order to eliminate the effect of the asymmetry inevitably involved in the actual practice, we measured the photosignals Q^+ and Q^- also in the opposite direction of magnetic field. We took $\frac{1}{2}[Q^+(+H_z)+Q^+(-H_z)]$ and $\frac{1}{2}[Q^-(+H_z)-Q^-(-H_z)]$ to be proportional to Q_x and Q_y.
[40]This is justified by the fact that the carrier range is negligibly small as compared with the specimen.
[41]The effect of acoustical-phonon scattering becomes noticeable for higher-purity samples or at higher lattice temperatures. See Ref. 15.
[42]R. B. Dingle, A. Arndt, and S. K. Roy, Appl. Phys. Sci. Res. B 6, 144 (1956); 6, 245 (1956).
[43]In the curve-fitting procedure, we implicitly assume that the quantities N and τ_t in Eqs. (1) and (2) do not vary with H_z. The excellent agreement of Q_x and Q_y to Eqs. (5) and (6) justifies this assumption.
[44]We adopt here Eq. (12) although the electron system is not in a thermal-equilibrium state. The numerical factor $\langle\tau\rangle^2/\langle\tau^2\rangle$ in Eq. (12) is 0.85 for $p=-\frac{1}{2}$ and 1 for $p=0$.
[45]F. C. Brown, T. Masumi, and H. H. Tippins, J. Phys. Chem. Solids 22, 101 (1961).
[46]See Eq. (8) in Ref. 66.
[47]In the following consideration, we assume that the quantity N is kept unchanged over the whole range of E_x and H_z. The quantity N will increase if impact ionization of trapped electrons is involved in the phenomena. The impact ionization, however, is believed hard to occur in the present experiment, since free electrons hardly acquire an energy enough for the impact ionization; the energy of free electrons is severely limited to $\hbar\omega_{LO}$ (23 meV for AgCl and 17 meV for AgBr), whereas the ionization energy of trapped electrons (36 meV for AgCl and 24 meV for AgBr) is larger than $\hbar\omega_{LO}$ (see Sec. IV D).
[48]The data of Q_x and Q_y at high E_x's are normalized by those at the lowest E_x.
[49]E. Conwell and V. F. Weisskopf, Phys. Rev. 77, 388 (1950).
[50]H. Brooks, Adv. Electron. Electron Phys. 7, 85 (1955).
[51]E. Hanamura, T. Inui, and Y. Toyozawa, J. Phys. Soc. Jpn. 17, 666 (1962).
[52]The constant $A=4.8\times10^{23}$ (erg sec)$^{-1}$ corresponds to the value of deformation potential, 4.5 eV.
[53]D. S. Tannhauser, L. J. Bruner, and A. W. Lawson, Phys. Rev. 102, 1976 (1956).
[54]See, for example, Ref. 2, p. 157.
[55]This seems to be a reasonable assumption for electrons (or holes) in silver halides. For example, compare the values of $\tau_{LO}^{-1}(\epsilon)$ in the energy range $\epsilon=1.1\,\hbar\omega_{LO}$ $\sim1.2\,\hbar\omega_{LO}$ (in Fig. 4) with the reciprocal of T_{LO} (in Table III).
[56]This is naturally expected from the magnitude of τ_{LO}^{-1} shown in Fig. 4. Also see K. K. Thonber, Phys. Rev. 133, 1929 (1971).
[57]For AgCl *M*1*CB* crystal ($p=-\frac{1}{2}$), τ_{imp} was calculated from the value of τ_{imp}^0 noted in Table I by the integration $(\tau_{imp})^{-1}=T_{LO}^{-1}\int_0^{T_{LO}}[\tau(\epsilon)]^{-1}dt$, where $\tau(\epsilon)=\tau_{imp}^0(\epsilon/kT)^{-1/2}$ and $\epsilon=\frac{1}{2}m^*[(eE_x/m^*)t]^2$. For the other crystals ($p=0$), $\tau_{imp}=\tau_{imp}^0$.
[58]The correct form of μ_H^s will be given in the Appendix [Eq. (A10)].
[59]Also note in Fig. 7 that the feature of the μ_H-E_x curve for the AgCl *M*1*CB* crystal is somewhat different from that of the other crystals; a gradual decrease in μ_H

begins at lower E_x and the gradual decrease continues up to relatively high E_x for AgCl *M1CB*. The equivalent feature is also noted in the $v_d - E_x$ curve (Fig. 9); the increase in v_d with E_x in an intermediate range of E_x (20–700 V/cm) is rather dull for this crystal. These behaviors of μ_H and v_d can be attributed to the nature of impurity scattering in this crystal ($p = -\frac{1}{2}$).

[60]This can be said for all the AgCl crystals, but not for AgBr crystals. In AgBr, a small contribution from holes makes it difficult to discuss the phenomena precisely.

[61]As a result, the (real) distribution of streaming electrons in the velocity space will become broad to some extent, forming a rod shape around the trajectory described in Fig. 21(a).

[62]Equivalent results were obtained by Voslyus and Levinson in Ref. 5.

[63]Equation (24) is equivalent to Eq. (4) in Ref. 6, where τ_{imp} in Eq. (24) corresponds to the acoustical-phonon scattering time $(W_{ac})^{-1}$ in Eq. (4) in Ref. 6.

[64]Both quantities $\tan\theta^s$ and V_y/v_x^s in Eq. (25) are functions of ξ. For example, $\tan\theta^s = 0.58$ and $V_y/v_x^s = 1.56$ for $\xi = 1.4$.

[65]W. Zawazki, *Physics of Solids in Intense Magnetic Fields*, edited by E. D. Haidemenakis (Plenum, New York, 1969), pp. 307–327.

[66]R. S. Van Heyningen and F. C. Brown, Phys. Rev. 111, 462 (1958).

[67]R. C. Brandt and F. C. Brown, Phys. Rev. 181, 1241 (1969).

[68]S. Sakuragi and H. Kanzaki, Phys. Rev Lett. 38, 1302 (1977).

[69]Thermal generation of trapped electrons to the conduction band becomes noticeable in the temperature range above 23 K (AgCl) and 17 K (AgBr); a long decay component of the photocurrent (with decay time 100 μsec–5msec) ascribed to the thermal generation of trapped electrons appears after the pulsed photoexcitation.